UNIVERSITY OF CALIFORNIA, SAN DIEGO

The Biophysical Diversity in Mutant p53DBD

A thesis submitted in partial satisfaction of the requirements for the degree

Master of Science

in

Chemistry

by

Jill Pailma Tee-Sy

Committee in Charge:

Professor Hector Viadiu, Chair
Professor Simpson Joseph, Co-Chair
Professor Jean Y. Wang

2014

A Thesis of Jill Tee-Sy is approved and it is acceptable in quality form for publication on microfilm and electronically:

_____

_____

Co-Chair

_____

Chair

Table of Contents

List of Figures

List of Tables

Acknowledgements

I would like to begin by thanking Dr. Hector Viadiu for giving me the opportunity to work his lab as an undergraduate and Masters student, which has brought me new experiences and memories that will not be forgotten. Without his guidance and persistent support, this thesis would not have been possible. I would especially thank my undergraduate mentors Sonha Nguyen and Dr. Abdul Ethayathulla who served to teach me valuable skills and pass down priceless knowledge in my early stages of research. I would also like to thank Ana Ramos who gave continuous support and challenged me with new knowledge and ideas constantly. To Kevin Lefever, I would like to thank you for the comic relief and wise tips you shared from past experiences. I would also like to thank past and current lab members, who all made my research experience enjoyable. I would like to especially thank John Lee for the patience and unending support when times were difficult.

ABSTRACT OF THESIS

The Biophysical Diversity in Mutant p53DBD

by

Jill Pailma Tee-Sy

Master of Science in Chemistry

University of California, San Diego, 2014

Professor Hector Viadiu, Chair

Professor Simpson Joseph, Co-chair

Tumor suppressor protein p53 plays a pivotal role in responding to the presence of cellular stress, where activation of p53 leads to induction of cell cycle arrest, DNA repair, and apoptosis. Mutations in p53 were present in 50% of cancer cases, where 95% of malignant tumors were caused by missense mutations in the DNA binding domain,

emphasizing its importance in cancer research. Recent studies have demonstrated the aggregations of p53 have the propensity of transforming into amyloid oligomers and fibrils, which were present in cancer cells. The goal of this thesis is to examine the diversity of mutant p53 DBD behaviors, specifically the recently observed amyloid fibril formation of p53 DBD, highlighting a new gain of function characteristic. To further assess the prion-like behavior of the amyloid fibrils, a seeding assay was conducted, which showed a gain of function, dominant negative effect of mutant p53DBD R248Q. The wild-type p53DBD and its mutant forms displayed the propensity to form amyloid fibrils with differing rates amongst each other. To supplement our understanding of the molecular basis of filament packing, structural studies of mutant p53DBD were conducted in order to examine the crystal packing, which showed evident differences in alignment and contacts within their unit cell. Examination of wild-type p73DBD capabilities to rescue mutant p53DBD proved to be inconclusive in a heterogeneous Thioflavin T fluorescence assay.

Chapter One

Introduction:

Cellular Function, Structure, Mutations, and Amyloid Fibril formation of Tumor Suppressor p53

1.1 Cellular Function of Tumor Suppressor Protein p53

The tumor suppressor p53 is a protein that functions as a transcription factor and it is regarded as the "guardian of the genome" because its central role in the cellular response to cellular stresses, in particular DNA damage (Levine 1997). When various cellular stresses occur, these events trigger the activation of p53 that prevents the proliferation of damaged cells (Levine and Oren 2009).

The transcriptional activity of p53 is regulated by a negative feedback loop that involves MDM2 and MDMX (Wade 2013). In normal cells, p53 induces the expression of MDM2, which eventually leads to the degradation of p53 (Picksley and Lane 1993). MDM2 possesses E3 ubiquitin ligase abilities and forms a heterodimeric complex with MDMX. The heterodimeric MDM2-MDMX complex binds to the N-terminus of p53 and polyubiquitinates the C-terminus of p53 (Alarcon-Vargas and Ronai 2001). MDMX is required for p53 interaction with and full induction of the MDM2 promoter after cellular stress (Biderman 2012). Consequently, the ubiquitination of p53 promotes the degradation of p53 by the proteasome in the cytoplasm (Vousden and Lou 2009). In addition, the binding of MDM2 to the N-terminus of p53 also inhibits its transcriptional activity (Momand et al. 1992).

The onset of various cellular stresses, such as DNA damage or metabolic stress, increases the cellular concentration of p53 and its post-translational modification. When the cell suffers stress, the heterodimer MDM2/MDMX is phosphorylated, it is unable to bind to p53 and it prevents the ubiquitination of p53, increasing its concentration (Xu 2003) (Harris and Levine 2005). At the same time, the activation of p53 also involves post-translational modifications, such as phosphorylation and acetylation (Xu 2003). The

decrease in degradation and the activating post-translational modifications account for the increased p53 concentration levels observed in stressed cells. Once the concentration of p53 increases, it plays an important role in the cellular response to stress by activating cell cycle arrest, DNA repair, and apoptotic pathways (Teodoro et al. 2007). Initially, p53 stops cells from dividing and induce DNA repair pathways, so DNA repair can occur. Once, DNA repair has failed, p53 induces cellular death to prevent the growth of severely damaged cells (Teodoro et al. 2007). The majority of active p53 is found in the nucleus acting as a transcription factor (Marchenko 2010). But, besides p53 activating proapoptotic genes and repressing prosurvival genes (Erster et. al 2004), it has been postulated that cytoplasmic p53 translocates to the mitochondria membrane binds Bcl and release cytochrome c that induces cellular apoptosis by activating caspases (Chipuk 2004).

1.2 Structure of Tumor Suppressor Protein p53

As the function of a protein is dictated by its structure, to understand the function of the p53 protein one must study its structure. The structure of the full-length p53 is comprised of the following domains: transactivation domain, proline rich region, DNA-binding domain, tetramerization domain, and C-terminus regulatory domain (Figure 1.1) (Viadiu 2008). The transactivation domain (TAD) lies in the N-terminal region of p53 and contains two subdomains: TAD1 (residues 1-40) and TAD2 (residues 41-61) (Lee et al. 2000). The TAD carries its transcriptional function by interacting with various transcriptional coactivators and corepressors (Jenkins 2012). As we mentioned, the E3 ubiquitin ligase heterodimeric complex MDM2/MDMX interacts with the N-terminal

region of p53, specifically with the transactivation domain, to negatively regulate p53 (Teufel et al. 2007). In addition, the p53 TAD also interacts with CBP/p300 and other various transcriptional coactivators to trigger CBP/p300 mediated transcription (Avantaggianti et al. 1997). To optimally accomplish its recruiting function, the structure of the p53 TAD is intrinsically disordered as NMR studies have shown (Dawson et al. 2003). In the absence of binding partners, the p53 TAD displays weak secondary structure with a helical conformation between residues 18 and 26 and turns at residues 40-44 and 48-53 (Lee et al. 2000). Once p53 binds to target proteins, the helices in TAD1 and TAD2 become more stable (Lee et al. 2000). In addition, the TAD is also phosphorylated during p53 activation, blocking p53 from interacting with MDM2/MDMX (Wang and Eckhart 1992).

Adjacent to the TAD, the proline rich domain (PRD) consists of residues 61 to 92 and lies between the transactivation domain and the DNA-binding domain. The PRD contains 5 repeats of a PXXP motif, where X represents non-proline amino acids (Venot et al. 1998). The PRD role is poorly understood, but there are studies that suggest a role in regulating the activation of cell death pathways (Baptiste et al. 2002).

The DNA-binding domain (DBD) spans from the residue 93 to the 292 (Figure 1.1). This domain consists of a β-immunoglobin-like sandwich that provides the structure to recognize specific DNA sequences (Cho 1994). Both β-sheets are formed by antiparallel β-strands. One β-sheet consists of four β-strands (S1, S3, S5, S8) and the other of five β-strands (S4, S6, S7, S9, S10) (Cho 1994). There are two α-helices in the DBD, H1 and H2, which are on the surface of the structure, one helps in the dimerization of two DBDs, while the other directly recognizes the DNA sequence. In addition, there

are three loops, L1 (residues 112-124), L2 (164-194), and L3 (237-250) (Figure 1.3a)(Joerger and Fersht 2010). The protein surface that binds to the DNA major groove is formed by loop L1 and helix H2, and some residues in loops L2 and L3 bind to the DNA minor groove (Figure 1.3b). The conformation of loops L2 and L3 is stabilized by a Zn^{2+} ion that it is hold by four residues (H179, C176, C238, and C242) (Cho 1994). The Zn^{2+} ion plays an important role in providing the structure thermodynamic stability, as the lack of the Zn^{2+} ion induces aggregation and lack of sequence specificity recognition (Jenkins 2012).

The tetramerization domain (TD) is located after the DBD from the residue 325 to the 356. The TD regulates oligomerization and enhances DNA-specificity (Chene 2001). The TD is a dimer of dimers with each monomer having a β-strand and an α-helix (Jeffrey et al. 1995). Each dimer is formed by one β-strand from each monomer forming an antiparallel β-sheet and an antiparallel helix-helix interface formed by the helix from each TD (Jeffrey et al. 1995). In the tetramer surface, two dimers interact with parallel helix-helix interface (Jeffrey et al. 1995).

The C-terminus regulatory domain (CTD) consists of residues 356 to 393. The CTD binds DNA non-specifically to DNA and it appears to regulate specific DNA binding by the DBD (Toledo and Wahl 2006). There are different hypotheses on the mechanism of how the CTD regulates the DBD. One view involves the existence of multiple p53 conformations that are dependent on the C-terminus (Ahn and Prives 2001). While the other hypothesis consists of p53 in two possible conformations for sequence-specific DNA binding, latent or active, which are allosterically regulated by the CTD (Ahn and Prives 2001). The structure of the CTD is intrinsically disorded, and like the

TAD, the CTD goes from a disordered to an ordered state upon DNA binding (Joerger and Fersht 2010). Moreover, the CTD also undergoes various post-translational modifications, such as acetylation, methylation, ubiquitination, sumoylation, neddylation at the carboxy-terminal lysines (Meek and Anderson 2009). In addition, the serine and threonine residues in both the TAD and CTD also become phosphorylated.

1.3 Mutations in p53 DNA-binding domain and its Relationship to Cancer

As we mentioned, the tumor suppressor p53 plays an important role in regulating cell cycle arrest, DNA repair, and apoptosis. Consequently, inactivation of p53 leads to tumor formation (Bosari 1994). The tumor suppressor p53 gene is found mutated in 50% of cancer cases, where 95% of malignant cases are due to missense mutations in the DNA binding domain (Toledo and Wahl 2006). Of those mutations, 80% of the mutations fall in amino acids called “hot-spot” residues. These “hot-spot” mutations occur at residues R175, Y220, G245, R248, R249, R273, and R282 (Figure 1.2) (Joerger and Fersht 2008). The missense mutations are divided into two classes: contact and structural mutants (Rolley 1995). The DNA contact mutants, such as mutations in R248 and R273, alter amino acids involved in DNA binding without affecting the overall protein structure; this category of mutations accounts for 20% of all cancer cases (Xu 2011). The structural mutants, such as mutations in residues R175, G245, R249 and R282, are critical for maintaining the stability of the tertiary structure of the protein and each modification destabilizes the overall structure in varying degrees; this category represents about 30% of all clinical cases (Xu 2011). Contact mutants do not display changes on thermodynamic stability (Joerger et al 2006). Instead, structural mutants affect the

thermodynamic stability of the protein in various degrees from 1 kcal/mol for the G245S mutant to 2 kcal/mol in R249S, and more than 3 kcal/mol for R282W (Joerger et al 2006). Mutations in the hydrophobic core of the β-sandwich can destabilize the structure by 4 kcal/mol, like mutations in Y220 (Joerger et al 2006).

Since the majority of the missense mutations in p53 occur in the core domain, there has been an emphasis in the structural understanding of the core domain and its mutant forms, the study of which would provide an overall insight into strategies to revert mutant p53 to its normal functioning state. However, some challenges have occurred in formulating a method to overcome certain commonly mutated residues in the DNA binding domain, in order to recover its native form. Specifically, mutations in residues R248 and R273 are exposed to solvent, rendering these two contact mutants not suitable drug targets due to the lack of a drug-binding cavity (Joerger 2005). In addition, structural determination of R175 has been difficult, due to its thermodynamic instability (Bullock 1997). Despite the challenges, progress has been made in recent studies by providing the following solutions: small molecule binding to increase stability, introduction of a second mutation, and mutating a p53-homolog with increased transactivation. The first method involved a small molecule which was able to bind in the cavity present in mutant Y220C, which induced the reactivation of mutant p53 (Liu 2014). The next solution consisted of introducing a second mutation at H168R to mutant R249S, which reestablished and re-stabilized the hydrogen bond network between loops L2A and L3 (Aguilar 1993). Lastly, mutation of a p53-homolog, like p73, has recently shown increased transactivation by simulating similar conformational binding to the same response elements p53 binds to (Ciribilli 2013).

Gain of function characteristics are present in mutated p53 in relation to tumorigenesis. Mutation in p53, most commonly found in the DNA binding domain, does not produce a loss of function in p53, as recent studies have shown the presence of mutated p53 in a p53 null cell induces tumorigenesis (Wolf et al. 1984). Likewise, a dominant negative effect is characteristic of this gain of function, where mutant p53 disrupts and inactivates native wild-type, by the formation of mutant/wild-type p53 cotetramers (Chan et al. 2004). Other gain of function features of mutant p53 involve the ability to retain wild-type p53 function, such as activating transcription from p53 response elements (Di Como and Prives 1998). In some cases, mutant p53 is also involved in inducing transcription of target genes that lead to varying biological effects, often producing an antagonistic effect on the cell (Freed-Pastor and Prives 2012). In addition, mutant p53 has been shown to form aberrant protein complexes, which consequently alter cancer cell behavior (Song et al. 2007).

1.4 Characterization of the Amyloid Fibril Formation of p53

Proteopathies can results from missense mutations that still yield a full-length protein produce loss-of-function and gain-of-function mutants. In the first group, the loss-of-function mutants are found mutations that simply destroy the synthesis, transport, synthesis or stability of the protein rendering an inactive protein (Kopito and Ron 2000). Examples of these loss-of-function mutations are found in the chloride transporter of cystic fibrosis patients or in proteins of the cholesterol pathway in hypercholesterolaemia patients. In the second group, the gain-of-function mutants result in the misfolding of proteins that lead to protein conformational diseases where the accumulation of protein

aggregates in the cell results in the onset of the disease. Examples of the gain-of-function mutations are found in the amyloids of Alzheimer and Parkinson disease (Kopito and Ron 2000).

In recent studies, proteins that typically were not associated in causing protein conformational diseases have been found to display the propensity to form amyloid fibrils (Harrison 2007). Missense mutations inactivate p53 in 50% of cancer cases (Toledo and Wahl 2006). The comparison between p53 knock-out and mutant p53 knock-in mouse experiments have strongly suggested that mutant p53 has a gain-of-function phenotype (Brosh and Rotter 2009).

Cancerous cells are known for accumulating large concentrations of mutant p53 in the nucleus (Rotter 1983). Native and inactive p53 are present in cancer cells, but high levels of inactive p53 tends to form aggregates (Sarnow et al. 1982). The current model describing the occurrence of aggregation in p53 DNA-binding domain involves the initial presence of native p53 in the nucleus and cytoplasm (Ishimaru et al. 2009). Eventually, p53 becomes inactivated and forms aggregates within the cytoplasm (Ishimaru et al. 2009). Native p53 in the nucleus eventually becomes transported into the cytoplasm, where aggregates present sequester native p53 and cause p53 to be inactive, as well as induce fibril formation (Figure 1.5) (Ishimaru et al. 2009). *In vitro* observations have suggested that that the high levels of mutant p53 form large aggregate deposits (Ishimaru et al. 2004). We think that both observations might be related and might help us to explain the gain-of function phenotype (Figure 1.6) (Lefever 2014). An example of this case would involve the frequently mutated DNA-binding domain residue R248. Mutations in R248 have been found in breast, colon, esophageal, gastric, lung, ovarian,

and prostate cancer, as well as leukemia (Ishimaru et al. 2004). When mutated, the residue R248 affects p53 ability to bind DNA and renders p53 incapable of preventing tumorigenesis, but at the same time it forms aggregates (Ishimaru et al. 2004). Mutant p53 might have a dual role, in one hand, it loses the DNA-binding function, but the aggregation of mutant p53 appears to contribute to negative dominance of mutant p53 leading to a gain-of-function phenotype (Figure 1.4) (Lasagna-Reeves et al. 2013).

In recent studies, the structure of amyloid fibril p53 has been analyzed. Circular dichroism and FTIR have shown that mutant p53 filaments have a larger proportion of β-sheet secondary structure than the native protein (Ano Bom et al. 2012). In addition, fiber diffraction experiments have shown diffraction at 4.7 Å and 10 Å that are typical of cross β-sheets (Ano Bom et al, 2012). The filaments have found to be able to enter cells and aggregate cytoplasmic wild-type p53 (Forget 2013).

Figure 1.1. **Domains of tumor suppressor p53**. Tumor suppressor p53 has five different domains. The first domain is the transactivation domain (TAD) with two subdomains, TAD1 and TAD 2. Following the TAD domain are the proline rich region (PRR), the DNA-binding domain (DBD), tetramerization domain (TD), and the C-terminal domain (CTD) (Viadiu 2008)

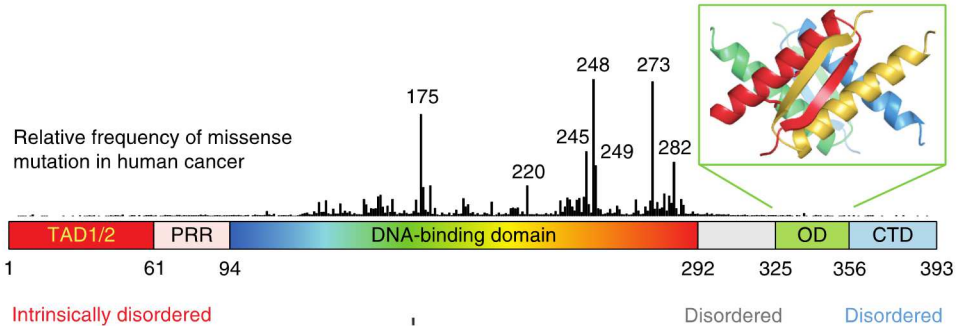

Figure 1.2. **Frequency of Missense Mutation in tumor suppressor p53**. Missense mutations occur frequently in the p53 tumor suppressor. The majority of these mutations are found in the DNA binding domain (Joerger and Fersht 2008).

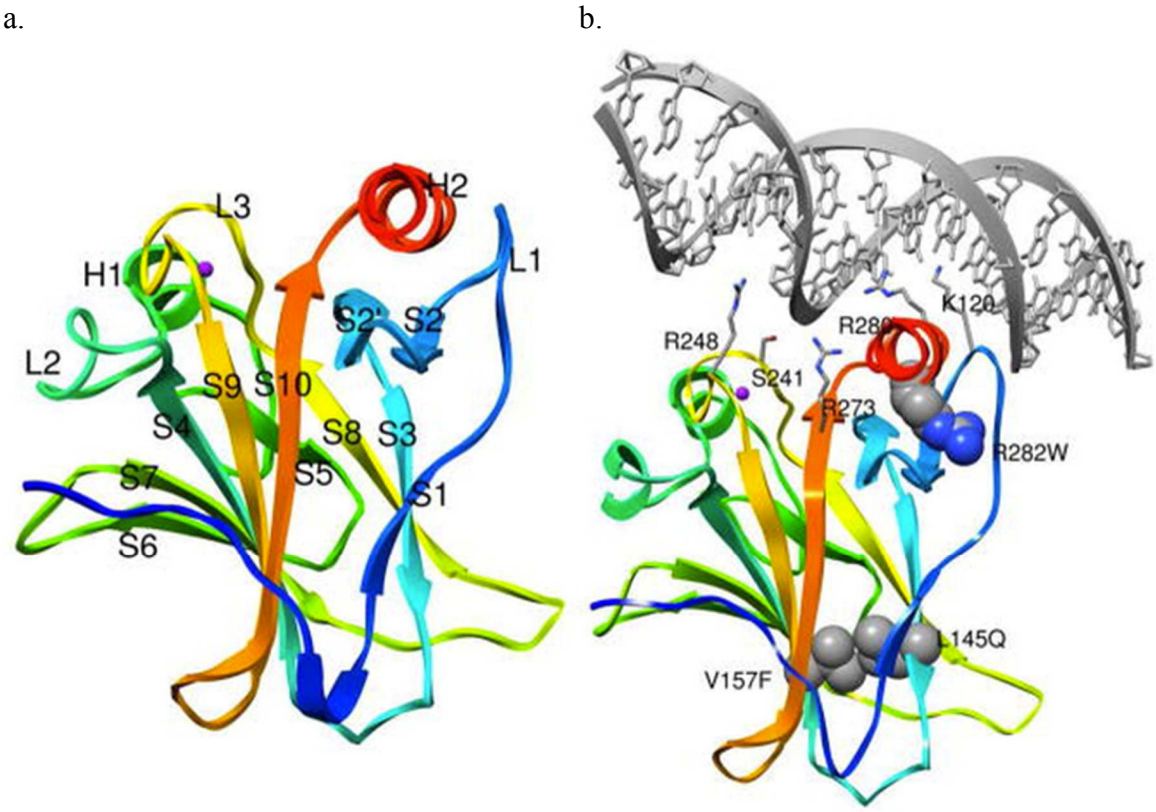

Figure 1.3. **Structure of p53 DNA-binding domain**. Crystal structure of wild-type p53 DBD is shown from the N-terminus (blue) to the C-terminus (red). (a) Crystal structure of wild-type p53 DBD without DNA. (b) Crystal structure of wild-type p53 DBD bound to DNA (Pavletich 1994).

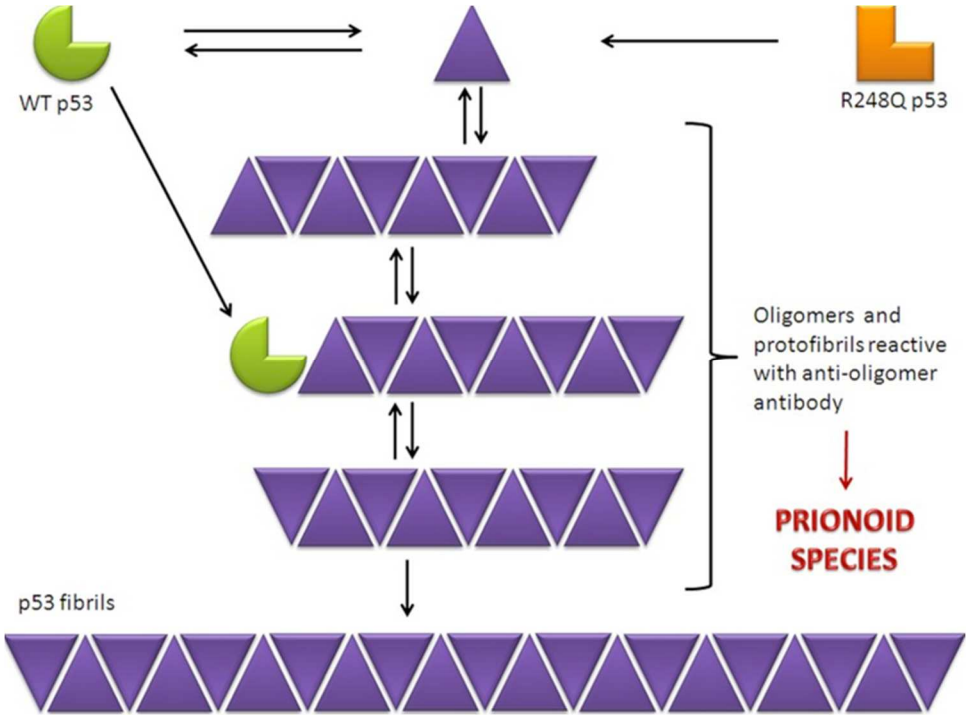

Figure 1.4. **Model of Prion-like behavior in p53 and Negative Dominance effect of mutant p53**. The misfolded mutant R248Q p53 (orange), which is prone to aggregation, eventually traps wild-type p53 (green). The prion-like behavior illustrate the dominant effect of mutant R248Q p53. (Ano Bom et al 2012)

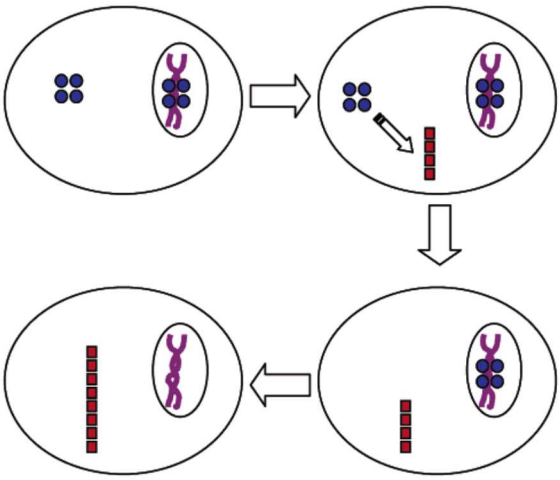

Figure 1.5. **Model of p53 aggregation in cell**. Native p53 (blue circles) are found in the cytoplasm and nucleus. Native p53 becomes misfolded forming fibrils (red squares). Native p53 in the nucleus is exported into the cytoplasm, where protofibrils inactivate and induce fibril formation. (Ishimaru et al. 2003).

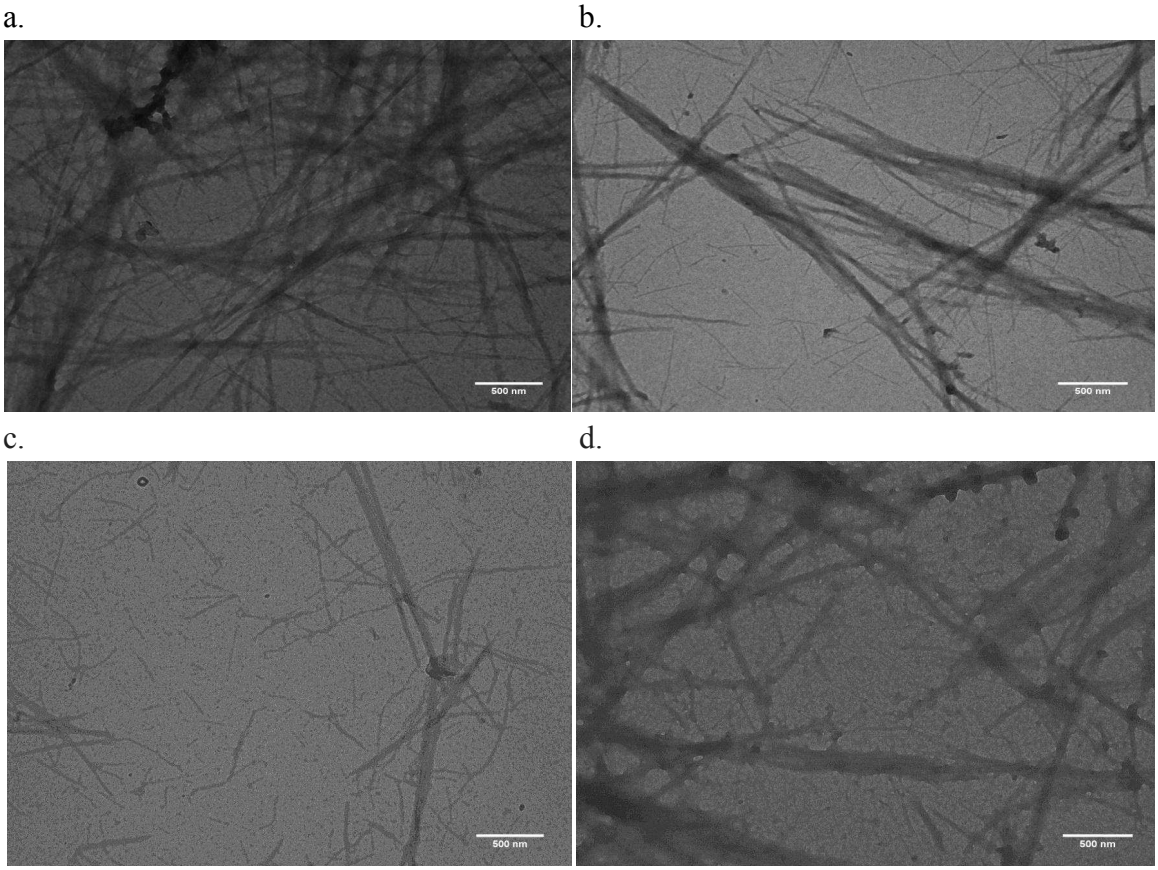

Figure 1.6. **TEM Micrographs of Amyloid Fibrils in mutant p53 DBD and wild-type p53 DBD.** The TEM images of mutant p53 DBD and wild-type amyloid fibrils were taken at 11,000x magnification. (a) R248Q p53 DBD. (b) R248S p53 DBD. (c) R273H p53 DBD. (d) wild-type p53 DBD. (Lefever 2014).

Chapter Two

Methods

2.1 Cloning of mutant p53 DNA binding domain

The Stratagene Quikchange site-directed mutagenesis protocol was used to generate all the studied mutations. The template for the mutagenesis experiments was a pET-28a vector containing a construct of the wild-type p53 DNA binding domain (residues 94 to 293) with an 8-His-tag in the N-terminus. Mutations in residues 103, 245 and 248 were generated. We created 8 plasmids carrying out single p53 mutations.

The plasmid product of the Quikchange reaction with mutant oligonucleotides was incubated for 1 hr with the restriction endonuclease DpnI at 37ºC to digest the original template that contained methylated adenine. 2 µl of the digested reaction were used to transform XL-1 Blue *E. coli* cells and grown in a LB-agar plate with 30 µg/ml of kanamycin as a selection marker. Plasmid was isolated from the surviving cells and sequenced to confirm the presence of the introduced mutations.

Table 2.1. **p53 DNA binding domain Mutants**. Mutations were introduced to pET-28a vector construct of the wild-type p53 DNA binding domain with an 8-His-tag in the N-terminus at specific residue sites.

Wild-type p53DBD Residue	**Introduced Mutation**	**Abbreviation**
Arg 248	Lys 248	R248K
Gly 245	Ser 245	G245S
Tyr 103	Ala 103	Y103A
Tyr 103	Lys 103	Y103K
Tyr 103	Asp 103	Y103E
Arg 248, Tyr 103	Glu 248, Ala 103	R248Q Y103A
Arg 248, Tyr 103	Glu 248, Lys 103	R248Q Y103K
Arg 248, Tyr 103	Glu 248, Asp 103	R248Q Y103E

2.2 Expression and Purification of mutant p53 DNA binding domain

Plasmids carrying the mutations to be studied were used to transform *E. coli* strain BL21 (DE3) using a heat shock protocol at 42ºC. Cells were grown in LB media with 30 µg/ml of kanamycin at 37ºC until an OD between 0.4 and 0.8 was reached. At that point,

1 ml of 0.5 mM isopropyl-β-D-thiogalactopyranoside per liter of culture was added to induce the expression of the chromosome-located T7 RNA-polymerase. Then the T7 RNA polymerase transcribed the plasmid-located mutant p53 DBD gene that is under the control of a T7 promoter. Cells were grown overnight at 25^{o}C and then pelleted down with a centrifugal force of 2,500xg. The pellet was resuspended in a lysis buffer containing 500 mM sodium chloride, 20 mM sodium citrate (pH 6.1) and 10 μM zinc chloride. An addition of 1 mM PMSF was introduced prior to cell lysis. The cells were then lysed using a microfluidizer and the cell lysate was centrifuged at 100,000xg at 4^{o}C for 30 minutes. The supernatant obtained was incubated overnight at 4^{o}C with 2 ml of Ni-NTA resin (Qiagen). Next day, the resin was washed with 200 ml of lysis buffer and 26 ml of lysis buffer containing 40 mM imidazole (pH 7.5). The protein was then eluted with lysis buffer containing 350 mM imidazole (pH 7.5). The imidazole was removed by desalting the protein with 150 mM sodium chloride, 20 mM sodium citrate (pH 6.1), 10 μM zinc chloride and 10 mM DTT. The protein was further purified by gel filtration chromatography using a superdex-200 column equilibrated with a 150 mM sodium chloride, 20 mM sodium citrate (pH 6.1), 10 μM zinc chloride and 10 mM DTT buffer. The mutant p53 DBD protein sample was concentrated to a 1 ml volume and loaded to the gel filtration column at a flow rate of 0.5 ml/min. The column was run at room temperature and monitored with a UV detector using a 280 nm wavelength. Fractions from the prominent elution peak were analyzed using a 15 % (w/v) SDS-PAGE that was stained with Coomassie blue. Fractions containing the target protein were then pooled together and concentrated. Besides the molecular weight observed in the SDS-PAGE, a

Western Blot using an anti-His-tag antibody was used. The same purification protocol was used for all studied mutants.

2.3 Thioflavin T Fluorescence Assay

A sample containing soluble wild-type p53 DNA binding domain at 5 μM and 25 μM thioflavin T was incubated at 37ºC and analyzed for 2 hours. This procedure was repeated for each mutant p53 DNA binding domain. The kinetics of filament formation of wild-type and mutants of p53 DNA binding domain was analyzed using a thioflavin T dye. Thioflavin T fluorescence was recorded with four measurements using polarized lenses in a Hitachi-F2000 fluorescence spectrophotometer with an excitation at 450 nm and an emission at 480 nm. The aggregation fraction was calculated using the following formula: aggregated fraction = $(F_{obs}- F_i)/(F_i-F_f)$, where F_{obs} represents the thioflavin T fluorescence emission intensity, F_i represents the initial thioflavin T fluorescence emission intensity, and F_f is the final thioflavin T fluorescence intensity.

2.4 Filament Seeding Assay

Filament formation was monitored measuring the thioflavin T fluorescence anisotropy using a Hitachi-F2000 fluorescence spectrophotometer with polarization lenses with an excitation at 450 nm and an emission at 480 nm. Mature aggregates of R248Q mutant p53 DNA binding domain were produced by incubating 20 μM R248Q p53DBD at 37ºC for 30 minutes. Afterwards, the R248Q p53DBD mature aggregates were diluted to 2 μM into a sample containing 5 μM of wild-type p53 DNA binding domain and 25 μM thioflavin T. This procedure was repeated for the wild-type p53 DNA binding domain wild-type, but using 10 μM to accelerate filament formation. The sample

was then incubated at 37ºC for 2 hours, fluorescence anisotropy was measured and the aggregation fraction was calculated. This protocol was also repeated using p73 DNA binding domain.

2.5 Thioflavin T Fluorescence of mutant R248Q p53 DBD with wild-type p73 DBD

Filament formation was monitored using thioflavin T fluorescence using Hitachi-F2000 fluorescence spectrophotometer with an excitation at 450 nm and emission at 480 nm. Soluble R248Q p53 DNA binding domain mutant at 5 μM and p73 DNA binding domain wild-type at 5 μM was incubated with 25 μM thioflavin T at 37ºC for 2 hours. The aggregation fraction was then calculated. This protocol was repeated using varying concentrations of p73 DNA binding domain wild-type at 1 μM, 10 μM, 15 μM, 20 μM.

Table 2.2. **Thioflavin T Fluorescence assay with wild-type p73 DBD and mutant R248Q p53 DBD.** Amyloid fibril formation of wild-type p73DBD in the presence of mutant R248Q p53 DBD were monitored using thioflavin T fluorescence. Varying concentrations of wild-type p73DBD were used with constant concentrations of mutant R248Q p53 DBD and Thioflavin T.

Assay #	[p73DBD wt]	[p53DBD R248Q]	[Thioflavin T]
1	1 μM	5 μM	25 μM
2	5 μM	5 μM	25 μM
3	10 μM	5 μM	25 μM
4	15 μM	5 μM	25 μM
5	20 μM	5 μM	25 μM

2.6 Crystallization of R248K p53 DBD and Y103K p53 DBD

R248K p53 DNA binding domain mutant was concentrated to 5 mg/ml and its crystallization was conducted using a VDX 24-well plate by the hanging drop vapor diffusion method. A mixture of 1 μl of the protein with 1 μl of the reservoir solution was placed in a coverslip that was sealed with vaseline over a well containing 1 ml of

reservoir solution. Optimal crystallization conditions were 14% PEG 3350, 0.3 M sodium chloride, 0.1 M bis-Tris methane (pH 6.4) at 23ºC. Crystals grew overnight. Prior to data collection, crystals were dipped into a cryoprotectant solution consisting of 25% PEG 3350, 0.3 M sodium chloride, 0.1 M bis-Tris methane (pH 6.4) and frozen using liquid nitrogen.

Y103K p53 DNA binding mutant was concentrated to 5 mg/ml and its crystallization was conducted using the same methodology employed in crystallizing R248K p53 DBD. Optimal crystallization conditions were 22% PEG 3350, 0.3 M sodium chloride, 0.1 HEPES (pH 7.2) at 23ºC. Crystals grew after a week. Prior to data collection, crystals were into a cryoprotectant solution consisting of 35% PEG 3350, 0.3 M sodium chloride, 0.1 M HEPS (pH 7.2) and frozen using liquid nitrogen.

2.7 Data Collection and Processing of R248K p53 DBD and Y103K p53 DBD

Crystals were diffracted in beamline 7-1 at Stanford Synchrotron Radiation Lightsource (SSRL), Palo Alto, California. Data sets were indexed, integrated and scaled using Mosflm (Leslie & Powell, 2007). The program Phaser (McCoy et al., 2007) was utilized to solve the structure of the R248K p53 DNA binding domain mutant. Molecular replacement conducted using Phaser using the previously solved structure of R248S p53 DNA binding domain mutant (resolution of 2.55 Å) as a starting model. The structure was further refined using PHENIX (Adams et al., 2010) and manually refined using Coot 0.7 (Emsley, 2004). Continuous cycles of refinement using PHENIX and Coot were conducted until R-free value was approximately 20%. The R248K p53 DNA binding domain mutant structure was validated using PROCHECK (Laskowski et al., 1993) and

figures were drawn with PyMOL Molecular Graphics System, Version 1.7, Schrödinger, LLC (DeLano, 2004). The same methodology was employed in solving the structure of Y103K p53 DBD with the exception of using the previously solved structure of R248Q p53 DNA binding domain mutant (resolution of 1.70 Å) during molecular replacement. Contacts between each monomer in respect to the center monomer for Y103K, R248K, R248Q (Lefever 2014), R248S (Lefever 2014), were analyzed using UCSF Chimera (Pettersen 2004).

Chapter Three

Filament Formation in p53 Mutants Frequently Found in Cancer Patients

3.1 Cloning of Mutant p53 DNA Binding Domain

The overexpression plasmids carrying the gene for the studied p53 DNA binding domain mutants originated from modifications to a pET28 plasmid carrying wild-type human p53 DBD with a N-terminus His-tag. The 5.8 kbp expression vector pET-28a displayed in Figure 3.1 included the mutant p53 DNA binding domain gene under a T7 lac promoter, the His-tag and the kanamycin gene for selection. Mutations were introduced by a Quikchange site-directed mutagenesis protocol. We created the following mutations: R248K, G245S, Y103A, Y103K, Y103E, R248Q/Y103A, R248Q/Y103K and R248Q/Y103E. Mutations R248K and G245S were used to demonstrate characteristics of missense mutations. The introduction of a second mutation in the context of the frequently mutated R248Q was due to the observation that Y103 makes crystal contacts with residue R248Q. To find a revertant mutant to the common R248Q mutation, we designed double mutants R248Q/Y103A, R248Q/Y103K and R248Q/Y103E aiming to delay the half-time of the aggregation reaction.

3.2 Acceleration of Wild-type p53 DBD Aggregation by Seeding with Aggregated R248Q

The assay of acceleration of aggregation by seeding required to prepare a mature amyloid fibril that would be considered the seed and to introduce this mature fibril into a sample containing soluble protein and Thioflavin T. The goal of the seeding assay was to determine if the rate of amyloid fibril formation accelerated when a mature fibril that could act as a filament seed was present. A sample of 20 μM R248Q p53 DBD mutant, in

a 50 µl volume, was incubated at 37ºC for 30 minutes in order to produce mature amyloid fibrils. The R248Q mutant was then diluted into a sample containing 5 µM soluble wild type p53 DBD and 25 µM thioflavin T. The mixture was incubated at 37ºC for 2 hours. Then the fluorescence anisotropy was measured at an emission of 480 nm, after exciting the sample at 450 nm. Using the values of fluorescence intensity, the aggregation fraction of the sample was calculated. The same assay was repeated using 10 µM wild-type p53 DBD. A sample with 5 µM soluble wild-type p53 DBD without R248Q seed was used as a control. As shown in Figure 3.7, the sample containing 2 µM R248Q seed with 5 µM wild-type p53 DBD, displayed a minimal shift in the rate of amyloid fibril formation and it overlapped with the control. While the mixture containing 10 µM wild-type p53 DBD with 2 µM R248Q seed displayed a visible acceleration in comparison to control and the seeded mixture with 5 µM wild-type p53 DBD.

The differences in the rate of amyloid fibril formation for each of the conducted wild-type p53 DBD seeded assays was analyzed according to the value of their half-life of thioflavin binding (thioflavin$_{(t1/2)}$). The values shown in Table 3.1 corresponded to the half-lives in the rate of fibril formation for the control and the seeded assays plotted in Figure 3.3. The seeded assay with 10 µM wild-type p53 DBD displayed a Th$_{(t1/2)}$ of 32 minutes in comparison to the sample with 5 µM wild-type p53 DBD that had a Th$_{(t1/2)}$ of 47 minutes. Both seeded wild-type p53 DBD assays displayed a lower Th$_{(t1/2)}$ than the control which lacked the mature mutant fibril, with a Th$_{(t/12)}$ of 52 min.

3.3 Do All the Frequently Found Cancer Mutants Form Filaments?: Thioflavin T Fluorescence Assays of the G245S, R248Q and R273H Mutants

The already described thioflavin T filament formation assay measured by fluorescence intensity was conducted for each of the three frequently found in cancer p53 DNA binding domain mutants to determine their propensity to form amyloid fibrils. As shown in Figure 3.8, each of the p53 DBD mutants was able to form amyloid fibrils, but their rate of amyloid fibril formation was different. The fastest rate of amyloid fibril formation was G245S, followed by R273H, and the slowest was R248Q. In an observation of potential biological importance, the three mutants showed a faster rate than the wild-type protein. In Table 3.2, the thioflavin$_{(t1/2)}$ binding half-lives represents the time in minutes that took for half of the protein to bind to the thioflavin T present. As thioflaving T is considered to only bind to the protein in the filament form, thioflavin$_{(t1/2)}$ value is considered as the time that it takes for half the protein sample to form filaments, in other words: the rate of fibril formation. The G245S p53 DBD mutant exhibited the fastest fibril formation rate because it has the lowest Th$_{(t1/2)}$ binding half-life. Instead, the R248Q p53 DBD mutant displayed the slowest rate of fibril formation among the three studied mutants. The slower rate of filament formation of the R248Q mutant represented an experimental advantage that allowed us to design experiments with the goal of understanding the molecular basis of filament formation.

3. 4 Is a Single Residue Promoting Filament Formation?: Thioflavin T Fluorescence Assays of the R248Q, R248S and R248K Mutants

Due to the avoidance of a very fast aggregation, we continue our studies with the R248Q mutant that allowed us to further characterize the tendency of p53 DBD mutants to form filaments. To determine whether the tendency of amyloid fibril formation was

specific to a single amino acid substitution, we studied three mutants with single amino acid mutations in the frequently mutated position R248. We conducted the fluorescence polarization thioflavin T binding assay for the R248Q, R248S and R248K p53 DBD mutants. As shown in Figure 3.9 and Table 3.3, each of the mentioned R248 mutants formed amyloid fibrils, although they differed in their rate of formation. From increasing order of rate of amyloid fibril formation consisted of the following: R248K, R248S, and R248Q. The R248K p53 DBD mutant exhibited the fastest fibril formation rate with the lowest $Th_{(t1/2)}$ binding half-life, followed by the R248S mutant and with the R248Q displaying the slowest fibril formation rate.

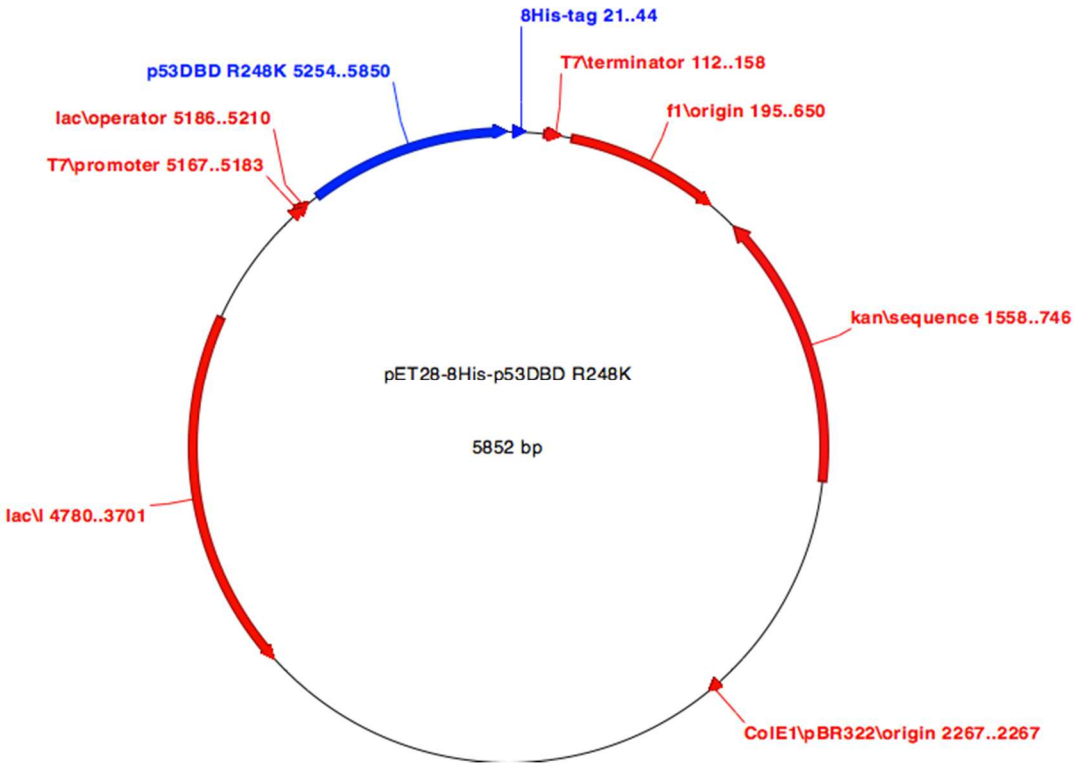

Figure 3.1. **Vector map of mutant p53DBD R248K**. Expression vector pET28-8His-p53DBD R248K contained an 8-His tag and kanamycin resistant gene. This vector was representative of the other mutants constructed with the exception of changes at different residues.

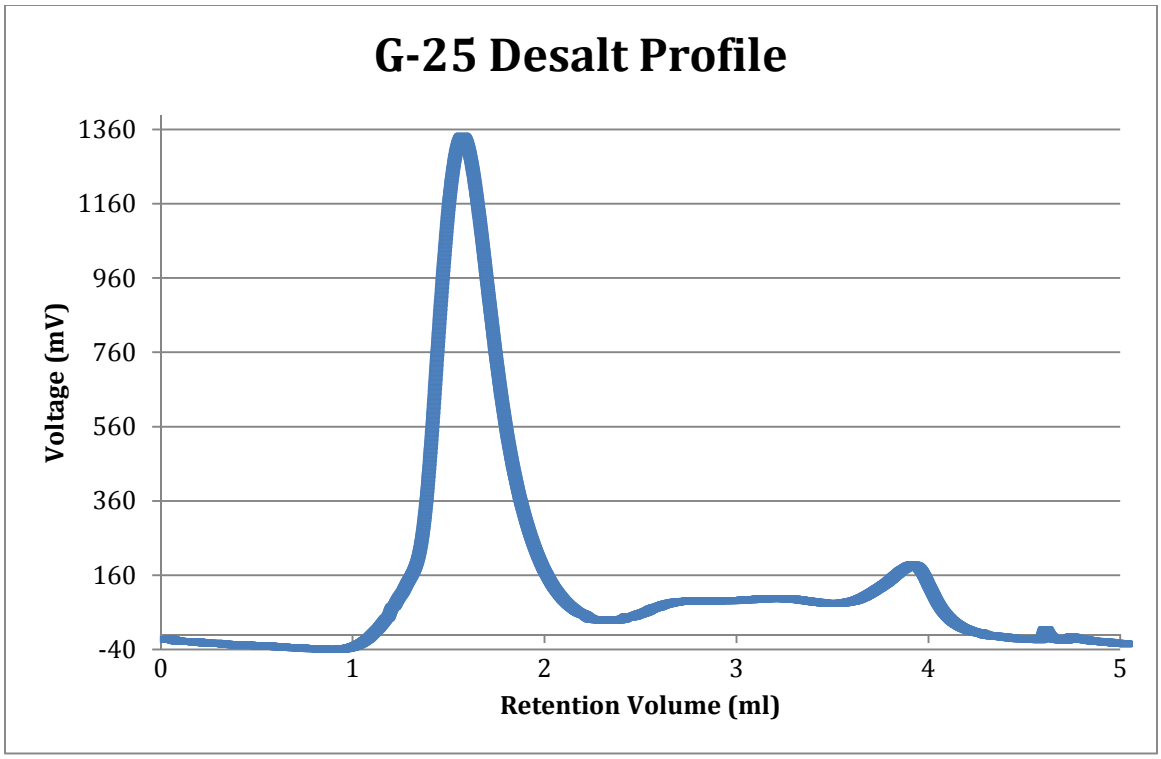

Figure 3.2. **G-25 Desalt Elution Profile**. Mutant p53 DNA binding domain was eluted from the G-25 column with 150 mM NaCl, 20 mM NaCitrate pH 6.1, 10 μM $ZnCl_2$, 10 mM DTT. The flow rate was at 1.5 ml/min and the absorbance was measured at 280 nm. Apparent separation of protein and imidazole was present.

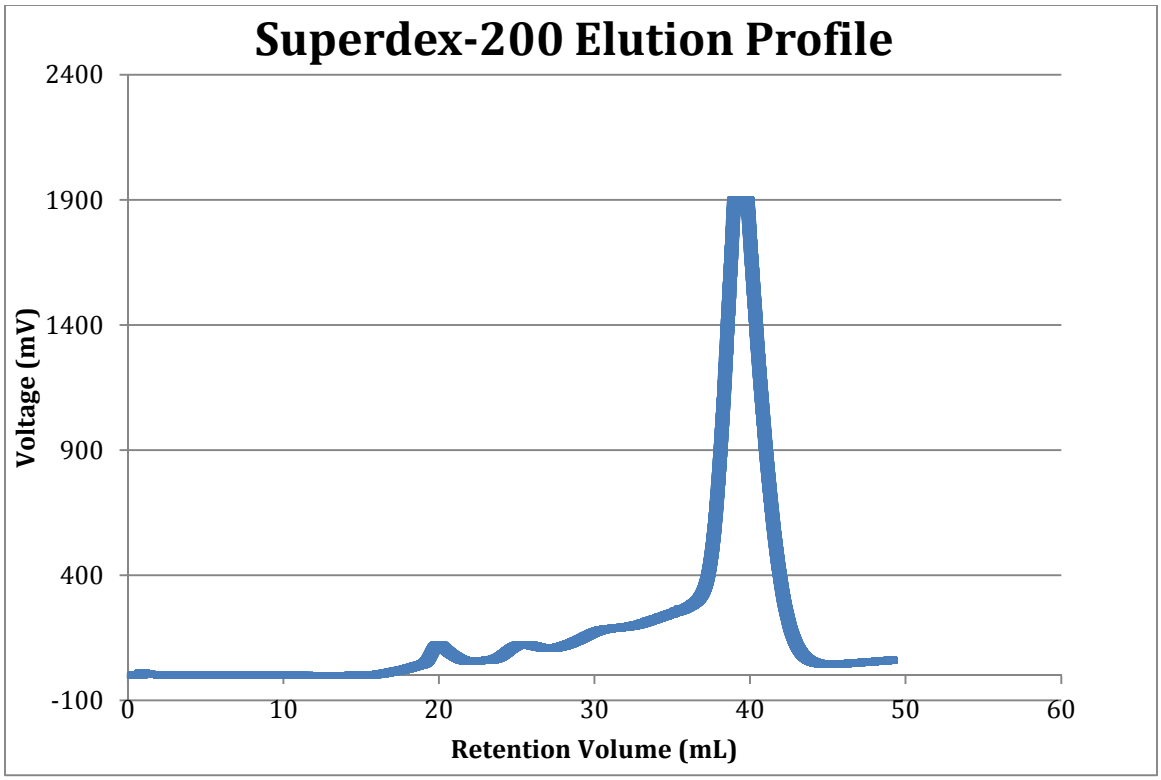

Figure 3.3. **Superdex-200 Elution Profile**. Mutant p53 DNA binding domain was further purified using a Superdex-200 gel filtration column. Protein was eluted with 150 mM NaCl, 20 mM NaCitrate pH 6.1, 10 μM $ZnCl_2$, 10 mM DTT. The flow rate was 0.5 ml/min and absorbance was monitored at 280 nm.

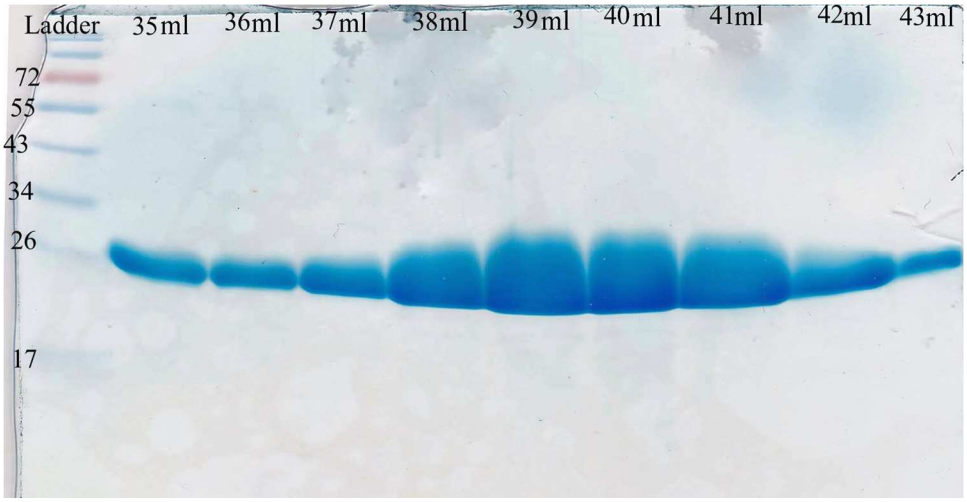

Figure 3.4. **SDS-PAGE of Gel Filtration Peak Fractions**. Fractions from elutions volumes 35 ml to 43 ml were analyzed using SDS-PAGE. Separation from high molecular weight contaminant proteins were apparent. Elution fractions displayed a molecular weight of 24 kDa, which corresponds to molecular weight of target mutant p53 DNA binding domain.

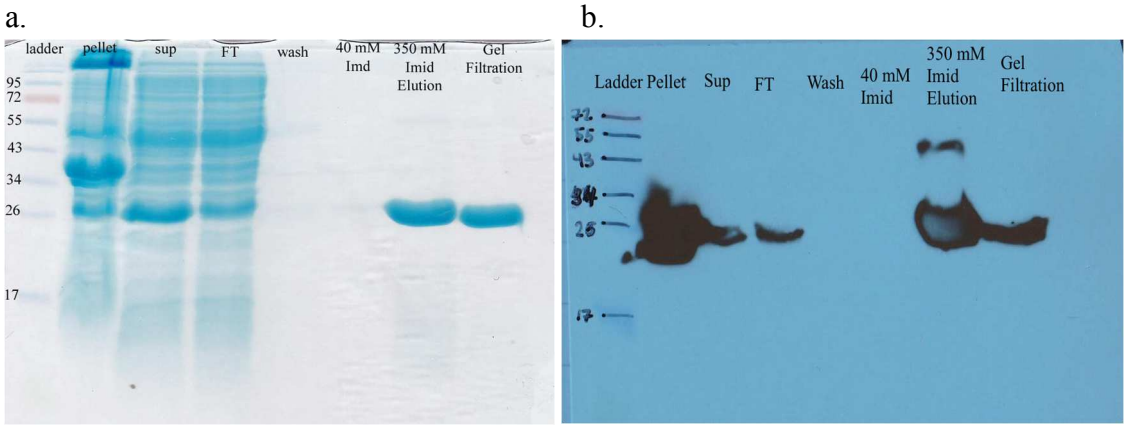

Figure 3.5. **Purification Scheme**. The purification scheme of mutant p53 DNA binding domain R248K was analyzed using SDS-PAGE, which displayed the purity of the sample from Ni-NTA and gel filtration chromatography. (a) The SDS-PAGE was stained using Coomassie stain. (b) A western blot of the purification scheme using anti-His antibody.

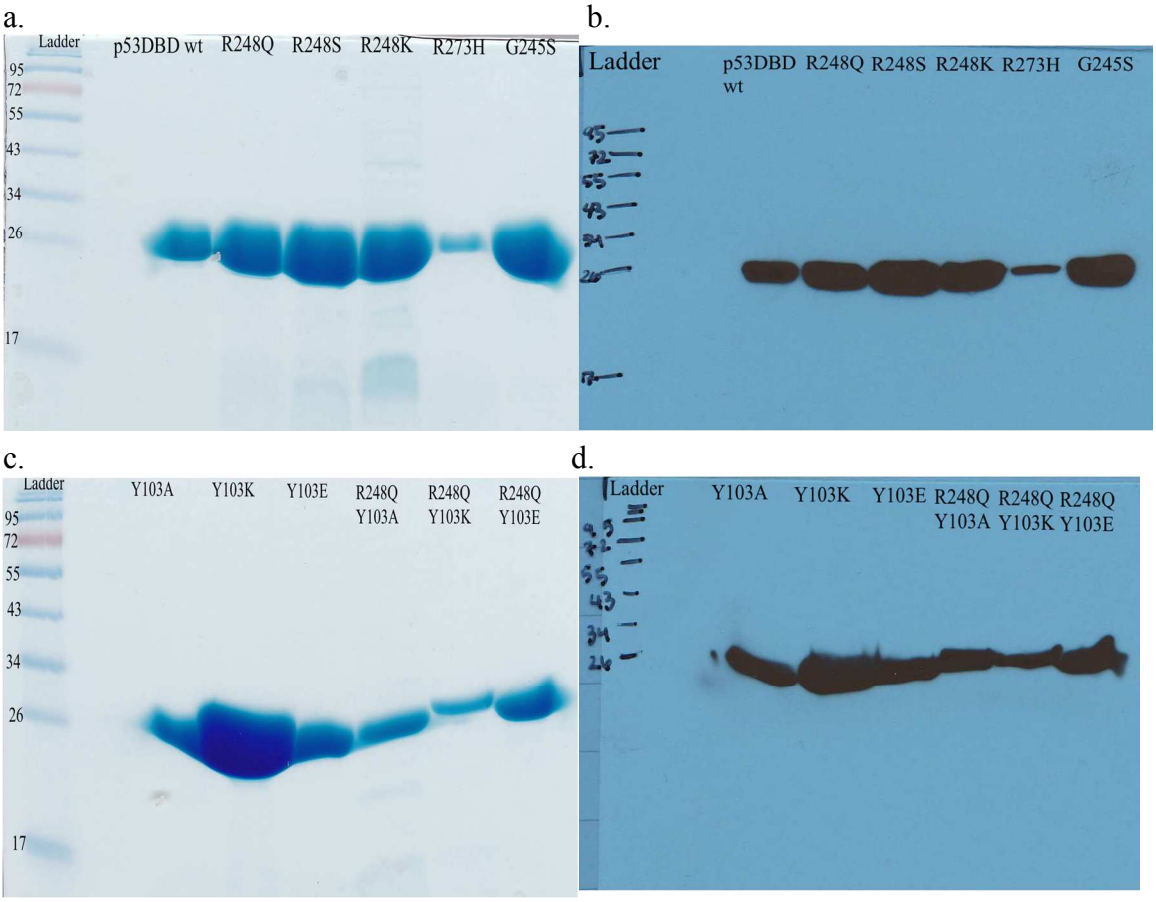

Figure 3.6. **Purified mutant p53 DNA binding domain**. SDS-PAGE analysis of the purity of the following: p53DBD wild-type, R248Q, R248S, R248K, R273H, G245S, Y103A, Y103K, Y103E, R248Q Y103A, R248Q Y103K, R248Q Y103E. Each mutant p53DNA binding domain displayed a molecular weight of 24 kDa and its 8-His tag was recognized by the anti-His antibody. (a, c) The SDS-PAGE was stained with Coomassie stain. (b, d) The western blot was conducted using anti-His antibody.

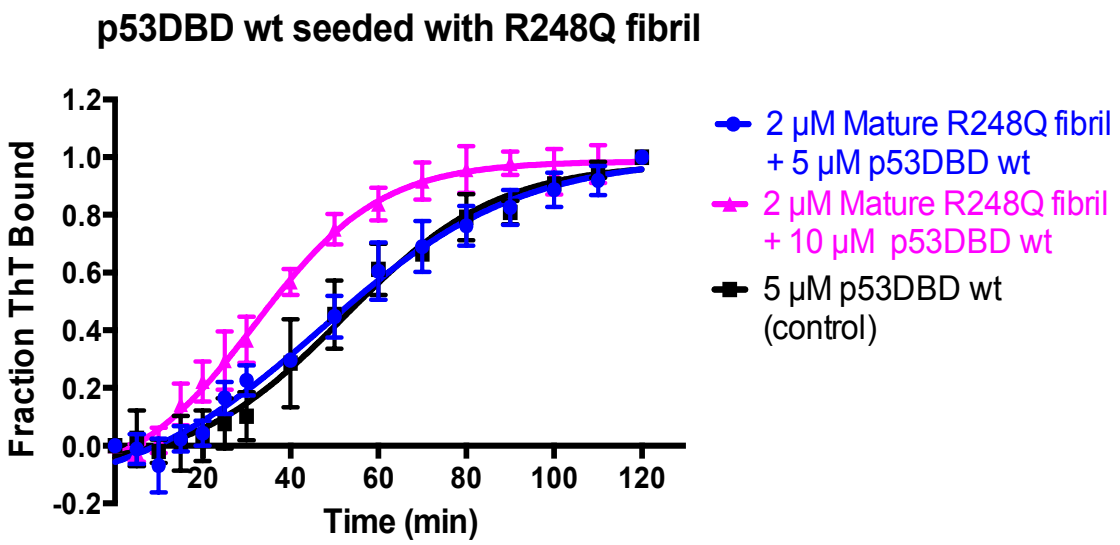

Figure 3.7. **Amyloid seeding assay of wild-type p53 DBD seeded with mutant R248Q mature fibrils**. Sample of 20 µM mutant R248Q p53 DBD was incubated at 37ºC for 30 minutes. R248Q fibrils were diluted to 2 µM in a sample also containing 5 µM soluble wild-type p53 DBD and 25 µM thioflavin T. The mixture was then incubated at 37ºC for 2 hours. Fluorescence intensity was measured at excitation of 450 nm and emission of 480 nm; from the values, the aggregation fraction was calculated. Seeding assay was repeated using 10 µM soluble wild-type p53 DBD. Wild-type p53 DBD without the seeded mutant fibril was used as a control.

Table 3.1. **Thioflavin$_{(t1/2)}$ Bound for Amyloid Seeding Assay**. The thioflavin$_{(t1/2)}$ bound, in minutes, was calculated for each seeding assay shown in Figure 3.7.

Mutant	ThT$_{1/2}$ Bound (min)
Seeded p53DBD wt (10 µM)	32
Seeded p53DBD wt (5 µM)	47
wild-type p53 DBD	52

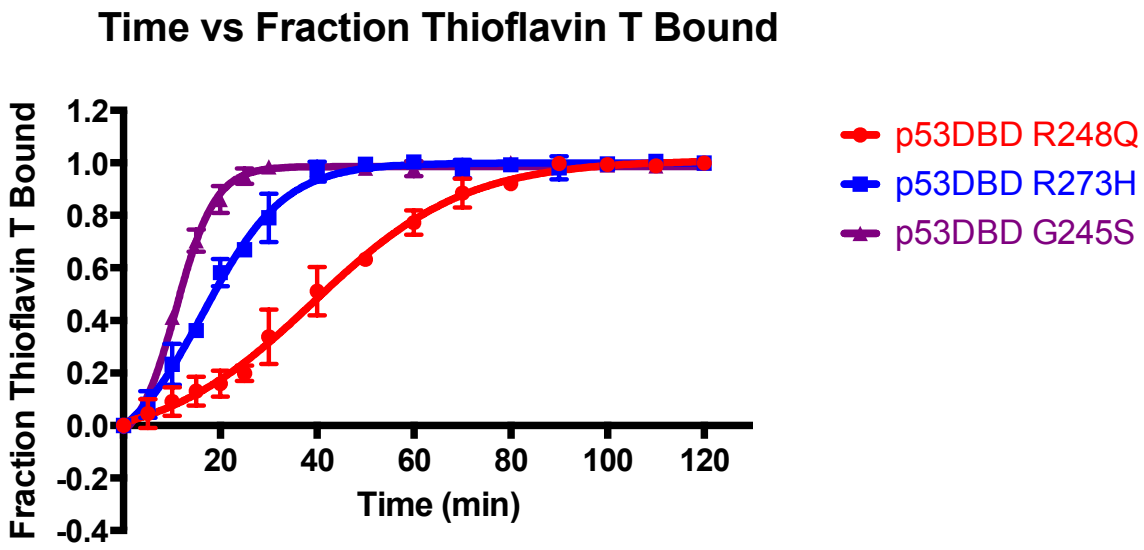

Figure 3.8. **Thioflavin T Fluorescence Assay**. The ThT assay was conducted with sample mixture containing 5 µM protein and 25 µM Thioflavin T, which was incubated at 37ºC for 2 hours. The fluorescence intensity was measured at an excitation and emission of 450 nm and 480 nm, respectively, the aggregation fraction was then calculated.

Table 3.2. **Thioflavin$_{(t1/2)}$ Fraction Bound**. The Th$_{(t1/2)}$ bound value, in minutes, was determined for each mutant shown in Figure 3.8. The Th$_{(t1/2)}$ bound value displayed the time it took for the sample to reach half of the fraction bound to ThT and half still in its folded state.

Mutant	ThT$_{1/2}$ Bound (min)
p53DBD G245S	11
p53DBD R273H	17
p53DBD R248Q	39

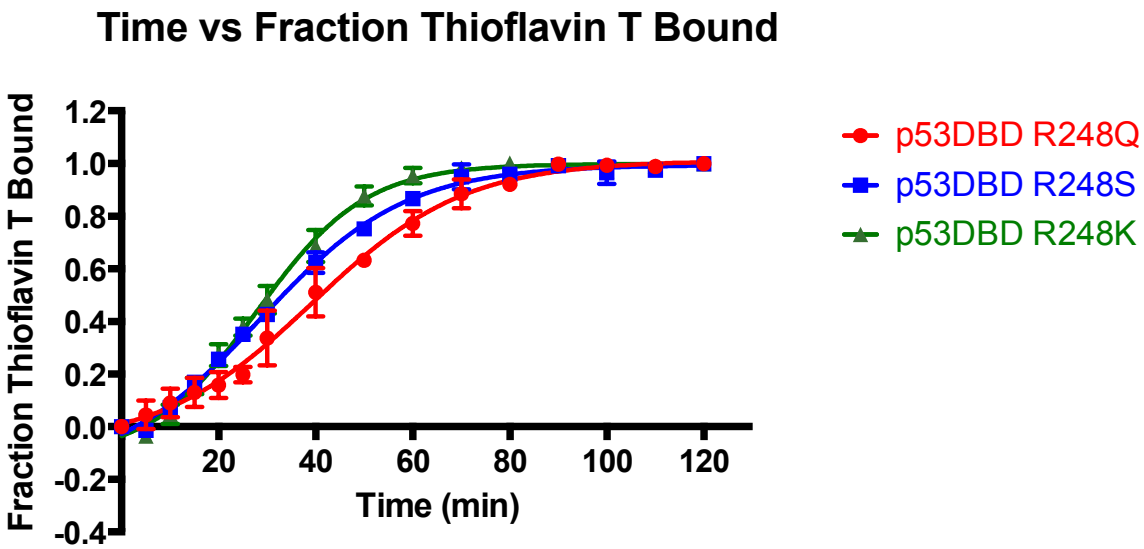

Figure 3.9. **Thioflavin T Fluorescence Assay of three R248 mutants**. The ThT assay was conducted with sample mixture containing 5 µM protein and 25 µM Thioflavin T, which was incubated at 37ºC for 2 hours. The fluorescence intensity was measured at an excitation and emission of 450 nm and 480 nm, respectively, the aggregation fraction was then calculated.

Table 3.3. **Thioflavin$_{(t1/2)}$ Fraction Bound**. The Th$_{(t1/2)}$ bound value, in minutes, was determined for each mutant shown in Figure 3.3. The Th$_{(t1/2)}$ bound value displayed the time it took for the sample to reach half of the fraction bound to ThT and half still in its folded state.

Mutant	ThT$_{1/2}$ Bound (min)
p53DBD R248K	28
p53DBD R248S	29
p53DBD R248Q	39

Chapter Four

Exploring the Molecular Basis of Filament Formation in the R248Q p53 Mutant

In order to understand the tendency of p53 DBD mutants to form filaments, we solved solved different crystal structures and analyzed their crystal packing aiming to shine light in possible explanations to the different tendencies of filament formation that might have physiological relevance in the gain-of-function activities of p53 mutants.

4.1 Crystal Packing Analysis in the Structures of the R248Q and R248S p53 DBD Mutants

In previous studies conducted by a former lab member, the structural determination of R248Q and R248S p53 DBD mutants suggested differences in the crystal packing due to differences in the unit cell dimensions of both crystal forms (Lefever 2014). I further examined the dimers present in the asymmetric unit of both crystals and I identified a similar alignment in one dimension, but packing was shifted in the other two dimensions (Figure 4.2). First, the arrangement of the monomers in the dimer found in each of the two crystals was similar, but it already indicated somewhat different crystal packing (Figure 4.1). To further analyze the packing, we used the dimer found in the asymmetric unit of both crystals and generated the surrounding symmetry-related molecules for the crystals of the R248Q and R248S p53 DBD mutants (Figure 4.3).

To define the crystal packing contacts, a monomer was taken as a reference and the contacts with the surrounding six monomers that contacted each monomer were analyzed for the R248Q and R248S p53 DBD crystals using UCSF Chimera (Pettersen 2004). For further description, we will refer to the reference monomer as the central

monomer and to the six surrounding ones as the top, bottom, front, back, left and right monomers. As shown in Table 4.1 and Table 4.2, contacts within each monomer pairs were categorized by the chemical nature: salt bridges for charge-charge interactions, hydrogen bonds for oxygen and nitrogen atoms that were in proximity of hydroxyl or amine groups and as Van der Waals interactions for non-polar atoms that were in close contact with other atoms. Table 4.3 compares the R248Q contacts from Table 4.1 with the R248S contacts from Table 4.2. Each interaction was categorized based on three criteria. The first criterion to judge crystal-packing similarity involved those contacts for the two monomers in the asymmetric unit. The second criterion involved contacts that were considered relative contacts involved intermonomer pairs where in one residue was conserved while the other interacting residue differed. And the third criterion consisted of different contacts that were not found in both mutant p53 DBD. For example in Table 4.1c and 4.2c, Arg 283 in center monomer is involved in contact with Arg 156 in side 2 monomer in both R248Q and R248S, while R248S has another interaction between Arg 283 in center monomer and Ser 260 in side 2 monomer.

Comparison of R248Q contacts with R248S contacts, seen in Table 4.3, displayed the prevalence of contacts found in monomeric interactions involving the center with side 2, side 4, and the bottom, respectively. The majority of these contacts were Van der Waals interactions (Table 4.3). These same monomer pairs had the most common contacts present in both mutants in each bond interaction category, the majority of which were Van der Waals interactions (Table 4.1 and Table 4.2). Minimal contacts were present when the center monomer interacted with the top, side 1, and side 3 monomer, respectively (Table 4.3). These same monomer pairs displayed the least number of

common contacts, where the majority of the contacts actually present between these monomer pairs were contacts present in one mutant monomeric unit cell but not the other (Table 4.1 and Table 4.2).

4.2 Crystallization of the R248K

The R248K p53 DBD mutant at a concentration of 5 mg/ml was crystallized with the hanging-drop vapor diffusion method in 14% PEG 3350, 0.3 M sodium chloride and 0.1 M bis-Tris methane (pH 6.4). Crystals grew overnight with a splitted-needle clusters appearance as seen in Figure 4.4.

4.3 Data Collection and Structure Determination of the R248K p53 DBD Mutant

For data collection, crystals were broken into single crystals prior to freezing. The crystals of the R248K p53 DBD mutant diffracted to 1.52 Å at the beamline 7.1 of the Stanford Synchrotron Radiation Lightsource. The methodological details can be seen in Chapter 2. Briefly, the structure of the R248K p53 DBD mutant was solved to a 1.52 Å resolution by molecular replacement using the R248S mutant as a search model. Crystals belonged to the $P2_1$ space group and they had two monomers per asymmetric unit, as shown in the data collection statistics in Table 4.4. For refinement in Phenix and Coot, 5% of the unique reflections (3082 reflections) were excluded to calculate the R_{free}. The final refinement statistics are shown in Table 4.5, which had a good stereochemistry with r.m.s. deviations of 0.006 Å for bond lengths and 1.075º for both angles.

4.4 Crystal Packing Analysis of the R248K p53 DBD Mutant

The packing of R248K p53 DBD mutant was analyzed by generating all the surrounding symmetry-related molecules in a sphere of 4 Å in Pymol (DeLano 2004). In Figure 4.5, the unit cell of R248K p53 DBD mutant dimers was constructed to illustrate a filamentous-like crystal packing. Dimeric mutant R248K p53 DBD itself was compared with dimeric R248Q p53 DBD and R248S p53, displaying similar alignment to both R248 mutants (Figure 4.6). Due to different cell dimensions present in mutant R248K p53 DBD (Table 4.4) compared to mutant R248Q p53 DBD and R248S p53 (Lefever 2014), this suggested the varying crystal packing abilities found in each R248 mutant. The packing was further analyzed by studying the monomeric unit cells of each mutant (Figure 4.7). The monomeric R248K unit cell was superimposed against monomeric unit cells of R248S and R248Q, respectively (Figure 4.7). In Figure 4.7b, the superimposition of R248K and R248S displayed similar structures with a visible slight shift between the two protein unit cells. However, in Figure 4.7c, the superimposition of R248K and R248Q displayed similar, but not identical structures with an apparent shift between the two protein unit cells for most of the monomers. An exception to this would be the top monomers, which instead of displaying an apparent shift when aligned, do not align at all.

Within the unit cell of R248K, the contacts were analyzed for each monomer in respect to the center monomer using UCSF Chimera (Pettersen 2004), in order to determine the crystal packing characteristics. As shown in Table 4.6, contacts within each monomer pairs were categorized by the following interactions: Van der Waals, hydrogen bonding, and salt bridges. The contacts were further compared to contacts found in the

R248S monomeric unit cell (Figure 4.3b) and R248Q monomeric unit cell (Figure 4.3a), where contacts within each interaction were analyzed based on three criteria, seen in Table 4.7 and Table 4.8. The first alignment criterion involved same contacts found within each monomer pair from each protein. Contacts that were considered relative contacts involved intermonomer pairs where in one residue was conserved while the other interacting residue differed. And the third criterion consisted of different contacts that were not found in both mutant p53 DBD.

Comparison of R248K monomeric unit cell with monomeric unit cells of R248S and R248Q displayed an increased number of contacts found when the center monomer interacted with side 2, side 4, and bottom monomer, respectively. According to Table 4.7 and Table 4.8, the majority of these contacts were Van der Waals interactions. These same monomer pairs exhibited the most common contacts found amongst the three R248 mutants in each category of bond interaction (Table 4.7 and Table 4.8). Two pairs of common contacts were present when the center monomer interacted with the side 1 monomer in mutant pairs R248K p53 DBD and R248S p53 DBD (Table 4.7), which was not present between R248K p53 DBD and R248Q p53 DBD (Table 4.8). Overall, minimal contacts were present when the center monomer interacted with the top, side 1, and side 3 monomers, respectively. These monomer pairs displayed the least number of common contacts (Table 4.7 and Table 4.8).

4.5 Crystallization of the Y103K p53 DBD mutant

The Y103K p53DBD mutant at a concentration of 5 mg/ml was crystallized using hanging-drop vapor diffusion method using 22% PEG 3350, 0.35 M sodium chloride and 0.1 M HEPES (pH 7.2). Crystals grew after a week with a needle cluster appearance (not shown).

4.6 Data Collection and Structure Determination of Y103K p53 DBD mutants

The crystals of Y103K p53DBD mutant diffracted to 1.85Å at the beamline 7.1 of the Stanford Synchrotron Radiation Lightsource. The same methodological details of solving the structure of R248K was employed in solving the structure of Y103K. The structure of Y103K p53DBD mutant was solved to a 1.85 Å resolution and molecular replacement was conducted using the monomer of the R248Q crystal structure as a search model. Crystals belonged to the $P2_1$ space group with two monomers per asymmetric unit, as shown in the data collection statistics in Table 4.9. For refinement in Phenix and Coot, 5% of the uniqe reflections (1607 reflections) were excluded to calculate the R_{free}. The final refinement statistics are shown in Table 4.10, displayed stereochemistry with r.m.s. deviations of 0.008 Å for bond lenghts and 1.086º for angle bonds.

4.7 Crystal Packing Analysis of the Y103K p53 DBD Mutant

The packing of Y103K p53 DBD mutant was analyzed by generating symmetry cells at one unit cell at 4 Å using Pymol (DeLano 2004). In Figure 4.8, the unit cell of Y103K p53 DBD mutant dimers was constructed to illustrate a filamentous-like crystal packing. Dimeric mutant R248K p53 DBD itself was compared with dimeric R248Q p53 DBD and R248S p53, displaying similar alignment to both R248 mutants (Figure 4.9).

Unit cell dimensions varied amongst the mutants, yet the mutants were grouped into two mutants pairs based on unit cell dimension similarities, where Y103K p53 DBD unit cell dimensions were similar to R248Q and R248K unit cell dimensions were similar to R248S (Table 4.9, Table 4.4) (Lefever 2014). These results suggest the two pairs have differing crystal packing ability. Upon examination of the filamentous packing, the assemblies between the two pairs differed, especially in the protein arrangement within the unit cell (Figure 4.8). These differences in packing are not readily apparent through visual examination of the dimers or the superimposition of the different mutant monomers (Figure 4.9 and Figure 4.10). The alignment of the monomers was similar along one axis, while the varied packing of the top and bottom monomers of the unit cell led to poor superimposition of those two monomers (Figure 4.10).

More work was then required to further analyze the monomeric unit cell and their residue contacts. Within the unit cell of Y103K, the contacts were analyzed for each monomer in respect to the center monomer using UCSF Chimera (Pettersen 2004), in order to determine the crystal packing characteristics. As shown in Table 4.11, contacts within each monomer pairs were categorized by the following interactions: Van der Waals, hydrogen bonding, and salt bridges. The contacts were further compared to contacts found in the R248K monomeric unit cell (Table 4.6), R248Q monomeric unit cell (Table 4.1), and R248S monomeric unit cell (Table 4.2), where contacts within each interaction were analyzed based on three criteria, seen in Table 4.12, Table 4.13, and Table 4.14. The first alignment criterion involved same contacts found within each monomer pair from each protein. Contacts that were considered relative contacts

involved intermonomer pairs where in one residue was conserved while the other interacting residue differed. And the third criterion consisted of different contacts that were not found in both mutant p53 DBD. Throughout each mutant, there were increased contacts and alignment along one axis, specifically the center monomer to side 2 and side 4, with a majority of those contacts being Van der Waals interactions (Table 4.12, Table 4.13, Table 4.14). Common contacts also only resided amongst these same monomer pairs, present in each bond interaction (Table 4.12, Table 4.13, Table 4.14). Minimal contact was present in Y103K from center monomer to top, side 1, side 3, and bottom monomers, respectively, in comparison to the three R248 mutants (Table 4.12, Table 4.13, Table 4.14).

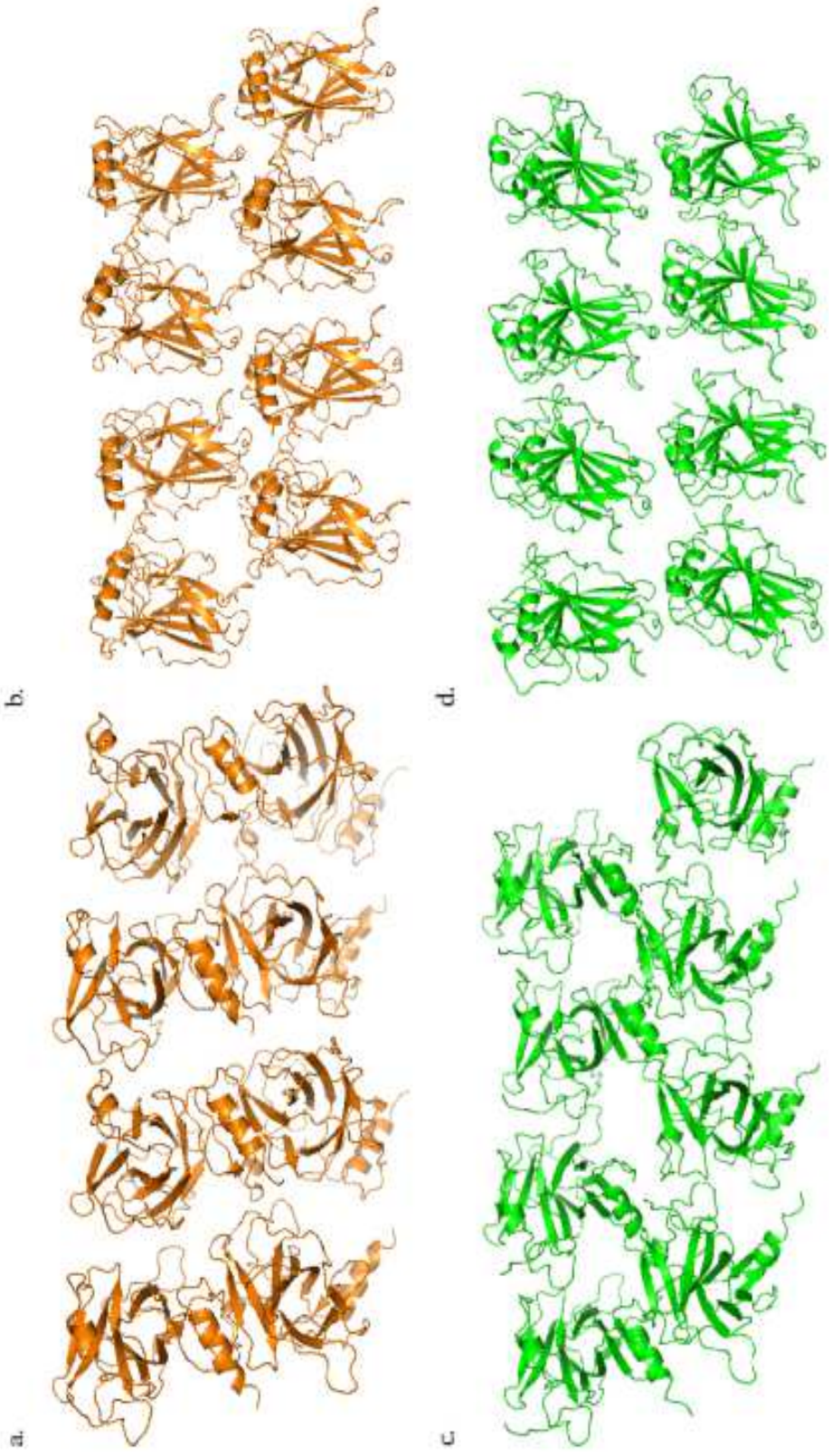

Figure 4.1. **Unit Cell of R248Q p53 DBD and R248S p53 DBD mutants.** The unit cell of dimeric R248Q p53 DBD and R248S p53 DBD mutant was constructed using Pymol (DeLano 2004). The unit cell was generated with symmetry mates at one unit cell within 4 Å. (a) Unit cell of R248Q p53 DBD in the x-y plane. (b) Unit cell of R248Q p53 DBD in the z-x

a.

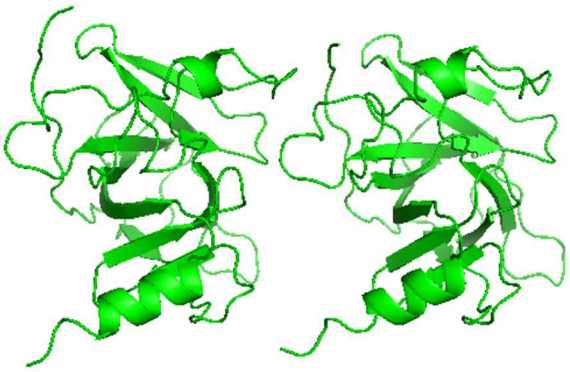

b.

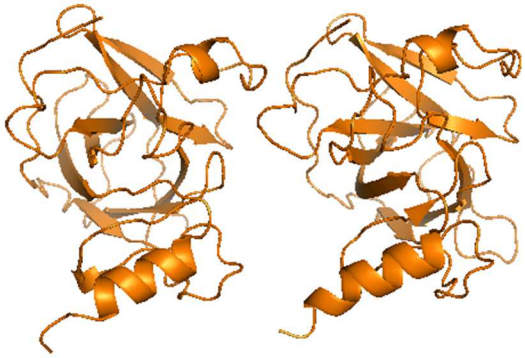

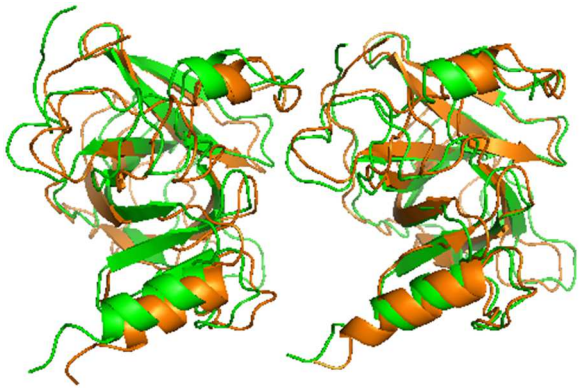

c.

Figure 4.2. **Structural Alignment of Dimeric Mutant R248Q p53 DBD and R248S p53 DBD**. The dimers of mutant R248Q p53 DBD and R248S p53 DBD were constructed using Pymol (DeLano 2004), using previously solved models of both mutants from a former lab member (Lefever 2014). (a) Dimeric R248Q p53 DBD. (b) Dimeric R248S p53 DBD. (c) Alignment of R248Q p53 DBD (green) with R248S p53 DBD (orange).

a. b.

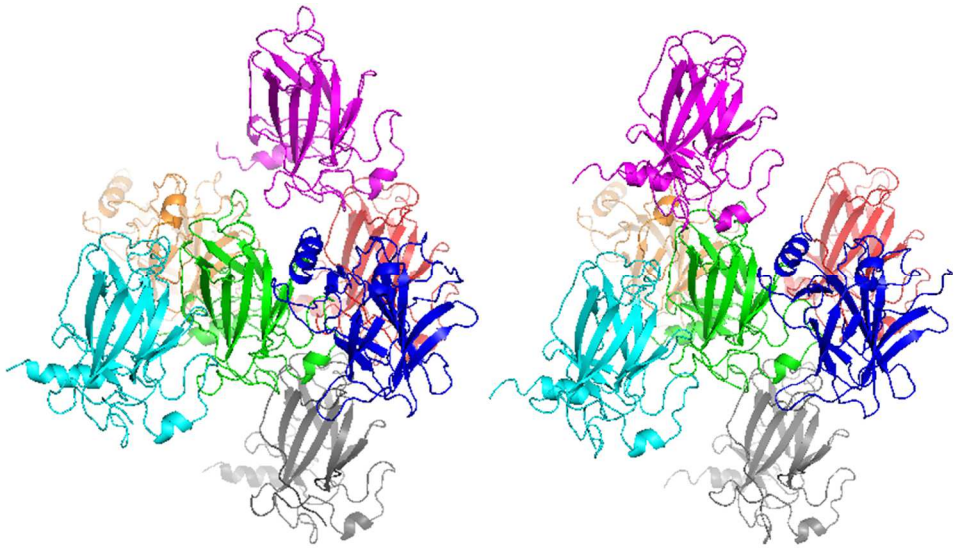

c.

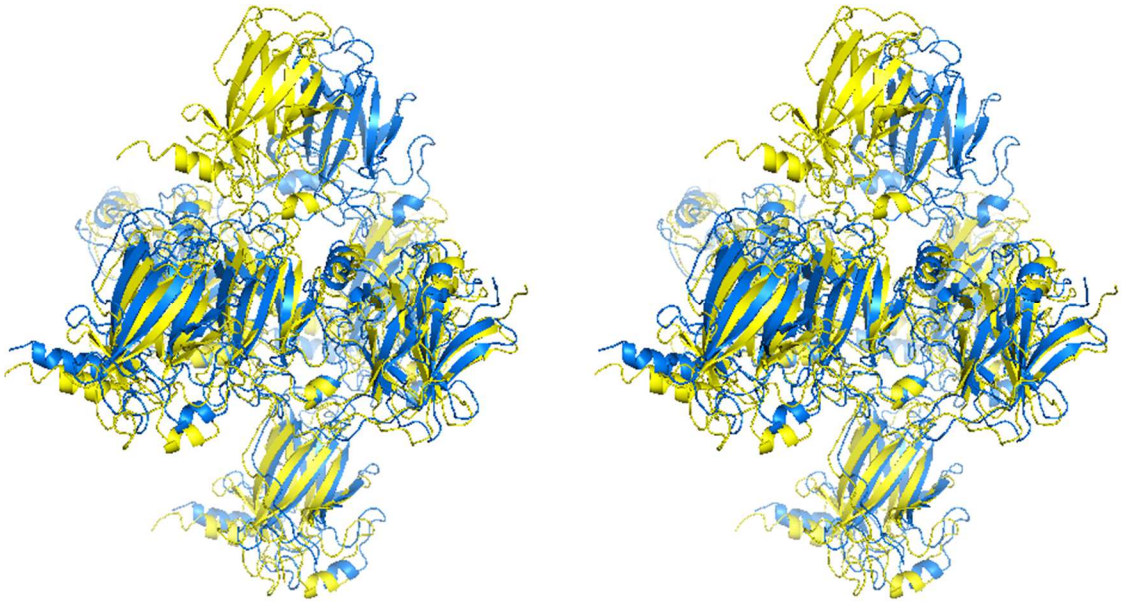

Figure 4.3. **Mutant R248Q and R248S Monomeric Unit Cells and their Structural Alignments.** The unit cell of R248Q and R248S monomers were constructed using Pymol (DeLano 2004) and aligned with each other. The unit cell consisted of monomers instead of dimers for the ease of visualization. (a) The R248Q monomers within the unit cell were designated by the following colors: top (magenta), center (green), side 1 (cyan), side 2 (blue), side 3 (red), side 4 (orange), bottom (grey). (b) The R248S monomers within the unit cell were designated by the same colors as the R248Q monomeric unit cell. (c) The stereoscopic image of R248Q unit cell (blue) superimposed with unit cell of R248S monomers (yellow).

Table 4.1. **R248Q contacts within Unit Cell.** Within the R248Q unit cell in Figure 4.3a, contacts were determined for each monomer in respect to the center monomer. Contacts were categorized into Van der Waals, hydrogen bonding, or salt bridge interactions.

a.

	Center Monomer	**Top Monomer**
Van der Waals	Glu 221	Gln 167
	Glu 224	Gln 167
Hydrogen Bonding	Glu 224	Gln 165
	Glu 224	Gln 167
Salt Bridges	None	None

b.

	Center Monomer	**Side 1 Monomer**
Van der Waals	Tyr 103	Glu 224
	Ser 106	Val 225
Hydrogen Bonding	Tyr 103	Glu 224
	Ser 106	Val 225
Salt Bridges	None	None

Table 4.1. (continued)

c.

	Center Monomer	Side 2 Monomer
Van der Waals	His 115	Pro 190
	His 115	Leu 206
	His 115	Asp 207
	Ser 116	Leu 206
	Thr 118	Glu 204
	Pro 128	Gly 187
	Pro 128	Leu 188
	Ala 129	Leu 188
	Arg 283	Arg 156
	Glu 286	Arg 202
	Glu 287	Arg 202
	Leu 289	Leu 201
	Lys 291	Gly 199
	Lys 291	Asn 200
	Lys 291	Leu 201
Hydrogen Bonding	His 115	Asp 207
	Thr 118	Glu 204
	Arg 283	Arg 156
	Arg 283	Ser 260
	Lys 291	Glu 221
Salt Bridges	His 115	Asp 207
	Lys 291	Glu 221

d.

	Center Monomer	Side 3 Monomer
Van der Waals	Lys 120	Lys 291
	Ala 138	Ser 166
	Ser 183	Phe 94
	Ser 183	Gln 167
	Ser 183	Thr 170
	Asp 184	Ser 166
	Gly 185	Thr 170
Hydrogen Bonding	Ser 183	Gln 167
	Ser 183	Thr 170
Salt Bridges	None	None

Table 4.1. (continued)

e.

	Center Monomer	Side 4 Monomer
	Arg 156	Arg 283
	Gly 187	Pro 128
	Leu 188	Pro 128
	Leu 188	Ala 129
	Pro 190	His 115
	Gly 199	Lys 291
	Asn 200	Lys 291
	Leu 201	Leu 289
	Leu 201	Lys 291
	Arg 202	Glu 286
	Arg 202	Glu 287
	Glu 204	Gly 117
	Glu 204	Thr 118
Van der Waals	Leu 206	Ser 116
	Asp 207	His 115
	Arg 156	Arg 283
	Leu 201	Lys 291
	Glu 204	Thr 118
Hydrogen Bonding	Asp 207	His 115
	Ser 260	Arg 283
Salt Bridges	Asp 207	His 115

f.

	Center Monomer	Bottom Monomer
	His 178	Tyr 107
	His 178	Pro 152
	His 178	Asp 259
	His 178	Asn 263
	His 178	Leu 265
	His 179	Ser 106
	Arg 181	Asp 259
	Arg 181	Ser 261
	Arg 181	Asn 263
	Ser 241	Tyr 103
	Ser 241	Gly 105
	Ser 241	Ser 106
	Cys 242	Ser 106
	Met 243	Tyr 103
	Met 243	Gly 266
	Met 243	Leu 264
	Met 243	Leu 265
Van der Waals	Asn 247	Tyr 103
	Gln 248	Tyr 103
	His 178	Tyr 107
	His 178	Asp 259
	Arg 181	Asp 259
	Arg 181	Asn 263
	Asn 239	Ser 106
Hydrogen Bonding	Ser 241	Tyr 103
	Asn 247	Tyr 103
Salt Bridges	His 178	Asp 259
	Arg 181	Asp 259

Table 4.2. **R248S contacts within Unit Cell.** Within the R248S unit cell in Figure 4.3b, contacts were determined for each monomer in respect to the center monomer. Contacts were categorized into Van der Waals, hydrogen bonding, or salt bridge interactions.

a.

	Center Monomer	**Top Monomer**
Van der Waals	None	None
Hydrogen Bonding	Ser 106	Arg 280
Salt Bridges	None	None

b.

	Center Monomer	**Side 1 Monomer**
Van der Waals	Lys 101 Tyr 103 Leu 264 Arg 267	Ser 227 Val 225 Glu 224 Glu 224
Hydrogen Bonding	Arg 267	Glu 224
Salt Bridges	Arg 267	Glu 224

Table 4.2. (continued)

c.

	Center Monomer	Side 2 Monomer
Van der Waals	His 115	Gln 192
	His 115	Pro 190
	His 115	Leu 206
	His 115	Asp 207
	Gly 117	Glu 204
	Thr 118	Glu 204
	Pro 128	Leu 188
	Ala 129	Leu 188
	Arg 283	Arg 156
	Arg 283	Ser 260
	Glu 286	Arg 202
	Glu 287	Arg 202
	Leu 289	Leu 201
Hydrogen Bonding	His 115	Asp 207
	Thr 118	Arg 156
	Thr 118	Glu 204
	Arg 283	Arg 156
	Arg 283	Ser 260
	Arg 287	Arg 202
	Arg 290	Arg 202
Salt Bridges	His 115	Asp 207
	Glu 286	Arg 202
	Glu 287	Arg 202

d.

	Center Monomer	Side 3 Monomer
Van der Waals	Phe 94	Gly 187
	Ser 166	Glu 198
	Thr 170	Asp 186
Hydrogen Bonding	None	None
Salt Bridges	None	None

Table 4.2. (continued)

e.

	Center Monomer	Side 4 Monomer
Van der Waals	Arg 156	Arg 283
	Leu 188	Pro 128
	Leu 188	Ala 129
	Pro 190	His 115
	Gln 192	His 115
	Leu 201	Leu 289
	Arg 202	Glu 286
	Arg 202	Glu 287
	Arg 202	Arg 290
	Glu 204	Gly 117
	Glu 204	Thr 118
	Leu 206	His 115
	Asp 207	His 115
Hydrogen Bonding	Arg 156	Thr 118
	Arg 156	Arg 283
	Arg 202	Arg 290
	Glu 204	Thr 118
	Asp 207	His 115
	Ser 260	Arg 283
Salt Bridges	Asp 207	His 115

f.

	Center Monomer	Bottom Monomer
Van der Waals	Pro 177	Asn 263
	His 178	Pro 152
	His 178	Asp 259
	His 178	Asn 263
	His 178	Leu 265
	Arg 181	Asp 259
	Arg 181	Ser 261
	Asn 239	Ser 106
	Ser 241	Tyr 103
	Cys 242	Ser 106
	Met 243	Tyr 103
Hydrogen Bonding	His 178	Tyr 107
	His 178	Asp 259
	Met 243	Tyr 103
Salt Bridges	His 178	Asp 259

Table 4.3. **Comparison of Contacts between R248Q unit cell (monomer) and R248S unit cell (monomer)**. Categorized contacts from each monomeric pair between R248Q and R248S unit cell, shown in Table 4.1 and 4.2 respectively, were analyzed. Within each type of interaction, the total unique contacts amongst the two unit cells were divided into the following: same contacts, relative contacts, or different contacts. The number of contact pairs and percentage were shown for each respective criteria
a.

Center Monomer - Top Monomer			
	Alignment Criteria	**Number of Contacts**	**% of Contacts**
Van der Waals	Same Contacts Pairs	0	0
	Relative Contact	0	0
	Different Contact Pairs	2	100
	Total	**2**	**100**
	Alignment Criteria	**Number of Contacts**	**% of Contacts**
Hydrogen Bonding	Same Contacts Pairs	0	0
	Relative Contact	0	0
	Different Contact Pairs	2	100
	Total	**2**	100
	Alignment Criteria	**Number of Contacts**	**% of Contacts**
Salt Bridges	Same Contacts Pairs	0	0
	Relative Contact	0	0
	Different Contact Pairs	0	0
	Total	**0**	**0**

Table 4.3. (continued)
b.

Center Monomer - Side 1 Monomer			
	Alignment Criteria	**Number of Contacts**	**% of Contacts**
	Same Contacts Pairs	1	20.0
	Relative Contact	0	0
Van der Waals	Different Contact Pairs	4	80.0
	Total	**5**	**100**
	Alignment Criteria	**Number of Contacts**	**% of Contacts**
	Same Contacts Pairs	0	0
Hydrogen	Relative Contact	0	0
Bonding	Different Contact Pairs	3	100
	Total	**3**	100
	Alignment Criteria	**Number of Contacts**	**% of Contacts**
	Same Contacts Pairs	0	0
	Relative Contact	0	0
Salt Bridges	Different Contact Pairs	1	100
	Total	**1**	**100**

c.

Center Monomer - Side 2 Monomer			
	Alignment Criteria	**Number of Contacts**	**% of Contacts**
	Same Contacts Pairs	10	55.6
	Relative Contact	6	33.3
Van der Waals	Different Contact Pairs	2	11.1
	Total	**18**	**100**
	Alignment Criteria	**Number of Contacts**	**% of Contacts**
	Same Contacts Pairs	4	50.0
Hydrogen	Relative Contact	1	12.5
Bonding	Different Contact Pairs	3	37.5
	Total	**8**	100
	Alignment Criteria	**Number of Contacts**	**% of Contacts**
	Same Contacts Pairs	1	25
	Relative Contact	0	0
Salt Bridges	Different Contact Pairs	3	75
	Total	**4**	**100**

Table 4.3. (continued)

d.

Center Monomer - Side 3 Monomer			
	Alignment Criteria	**Number of Contacts**	**% of Contacts**
Van der Waals	Same Contacts Pairs	0	0
	Relative Contact	0	0
	Different Contact Pairs	10	100.0
	Total	**10**	**100**
	Alignment Criteria	**Number of Contacts**	**% of Contacts**
Hydrogen Bonding	Same Contacts Pairs	0	0
	Relative Contact	0	0
	Different Contact Pairs	2	100.0
	Total	**2**	100.0
	Alignment Criteria	**Number of Contacts**	**% of Contacts**
Salt Bridges	Same Contacts Pairs	0	0
	Relative Contact	0	0
	Different Contact Pairs	0	0
	Total	**0**	**0**

e.

Center Monomer - Side 4 Monomer			
	Alignment Criteria	**Number of Contacts**	**% of Contacts**
Van der Waals	Same Contacts Pairs	11	64.7
	Relative Contact	4	23.5
	Different Contact Pairs	2	11.8
	Total	**17**	**100.0**
	Alignment Criteria	**Number of Contacts**	**% of Contacts**
Hydrogen Bonding	Same Contacts Pairs	4	57.1
	Relative Contact	1	14.3
	Different Contact Pairs	2	28.6
	Total	**7**	100.0
	Alignment Criteria	**Number of Contacts**	**% of Contacts**
Salt Bridges	Same Contacts Pairs	1	100.0
	Relative Contact	0	0
	Different Contact Pairs	0	0
	Total	**1**	**100.0**

Table 4.3. (continued)
f.

Center Monomer - Bottom Monomer			
	Alignment Criteria	**Number of Contacts**	**% of Contacts**
Van der Waals	Same Contacts Pairs	9	42.9
	Relative Contact	10	47.6
	Different Contact Pairs	2	9.5
	Total	**21**	**100.0**
	Alignment Criteria	**Number of Contacts**	**% of Contacts**
Hydrogen Bonding	Same Contacts Pairs	2	25.0
	Relative Contact	3	37.5
	Different Contact Pairs	3	37.5
	Total	**8**	100.0
	Alignment Criteria	**Number of Contacts**	**% of Contacts**
Salt Bridges	Same Contacts Pairs	1	50.0
	Relative Contact	0	0
	Different Contact Pairs	1	50.0
	Total	**2**	**100.0**

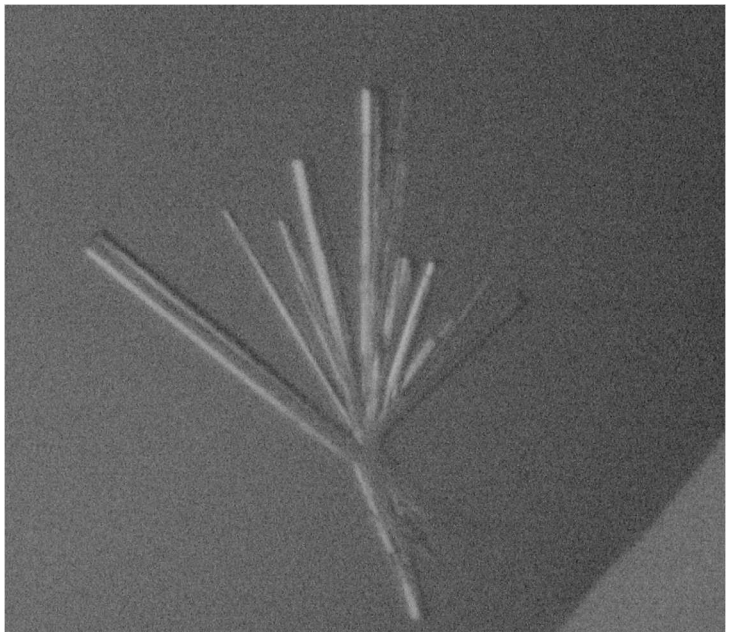

Figure 4.4. **R248K p53 DBD crystals**. Crystals were prepared with hanging drop vapor diffusion method with the condition 14% PEG 3350, 0.3 M NaCl, 0.1 M Bis Tris Methane pH 6.4.

Table 4.4. **Data collection statistics of R248K p53DBD**. The data collection statistics of p53DBD R248K was determined using Mosflm (Leslie and Powell 2007).

Data Collection	R248K p53DBD
Beamline	SSRL
Wavelength (Å)	1.27
Space group	1 2_1 1
Cell dimensions	
a, b, c (Å)	52.73, 68.42, 57.96
α=γ (º)	90
β (º)	98.9
Resolution (Å)	50-1.52
Rsym or Rmerge	0.045
I/σI	33.6 (4.6)
Completeness (%)	98.1 (96.8)
Redundancy	3.7 (3.7)

Table 4.5. **Refinement statistics of R248K p53DBD**. Refinement statistics of p53DBD R248K was determined using PHENIX (Adams et al 2010), Coot 0.7 (Adams et al 2010), PROCHECK (Laskowski et al 1993).

Refinement Statistics	p53DBD R248K
Refinement	
Resolution (Å)	28.591-1.43
No. reflections	73151
Rwork/Rfree	16.67/21.12
Molecules in A.U.	2
No. atoms	3727
Protein	3143
Zn^{2+} ion	2
Water	637
B-factors	25.49
Protein	25.49
Zn^{2+} ion	19.39
Water	40.12
R.m.s. deviations	
Bond lengths (Å)	0.006
Bond angles (º)	1.075
Dihedral angles (º)	12.972
Ramachandran Plot	
Most favored region	89.6
Additionally allowed region	10.1
Generously allowed region	0.3
Disallowed region	0

a.

b.

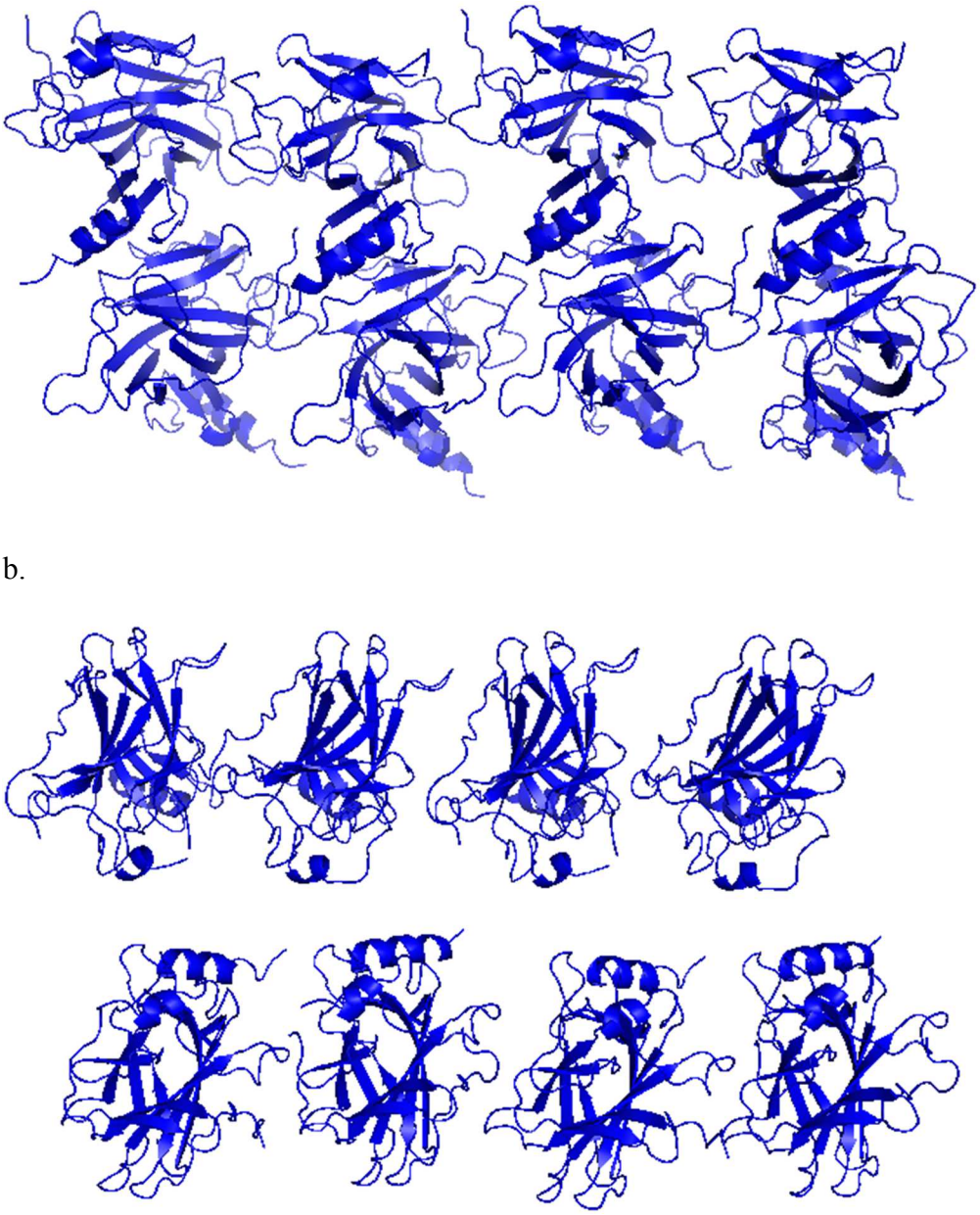

Figure 4.5. **Unit Cell of mutant R248K p53DBD**. The unit cell of dimeric mutant p53DBD R248K was constructed using Pymol (DeLano 2004). The unit cell was generated with symmetry mates at one unit cell within 4 Å. (a) Unit cell of R248K p53 DBD in the x-y plane. (b) Unit cell of R248K p53 DBD in the z-x plane.

a.

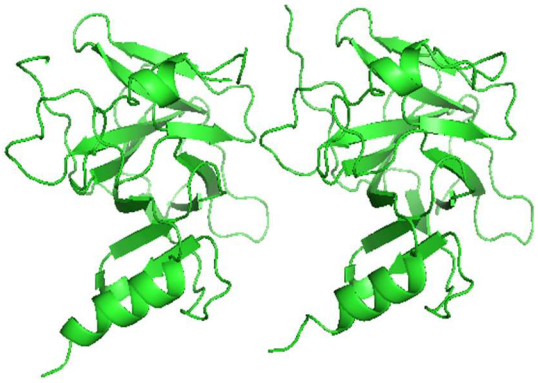

b.

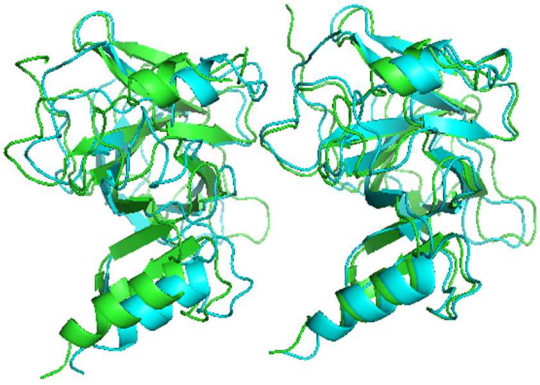

c.

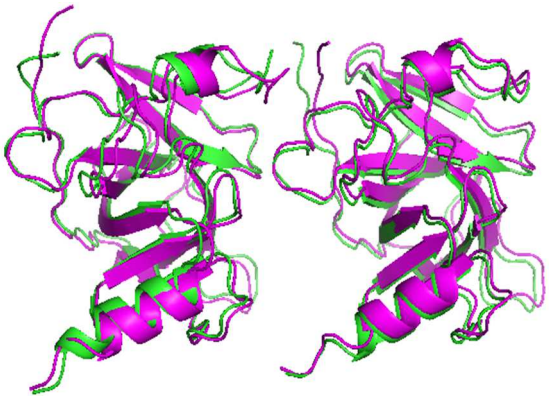

Figure 4.6. **Structural Alignment of Dimeric Mutant R248K p53 DBD with R248Q p53 DBD and R248S p53 DBD.** The dimer of mutant R248K p53 DBD was constructed using Pymol (DeLano 2004), which was superimposed with previously solved models of mutant R248Q p53 DBD and R248S p53 DBD from a former lab member (Lefever 2014). (a) Dimeric R248K p53 DBD. (b) Alignment of dimeric R248K p53 DBD (green) with dimeric R248Q p53 DBD (blue). (c) Alignment of R248K p53 DBD (green) with R248S p53 DBD (magenta).

a.

b.

c.

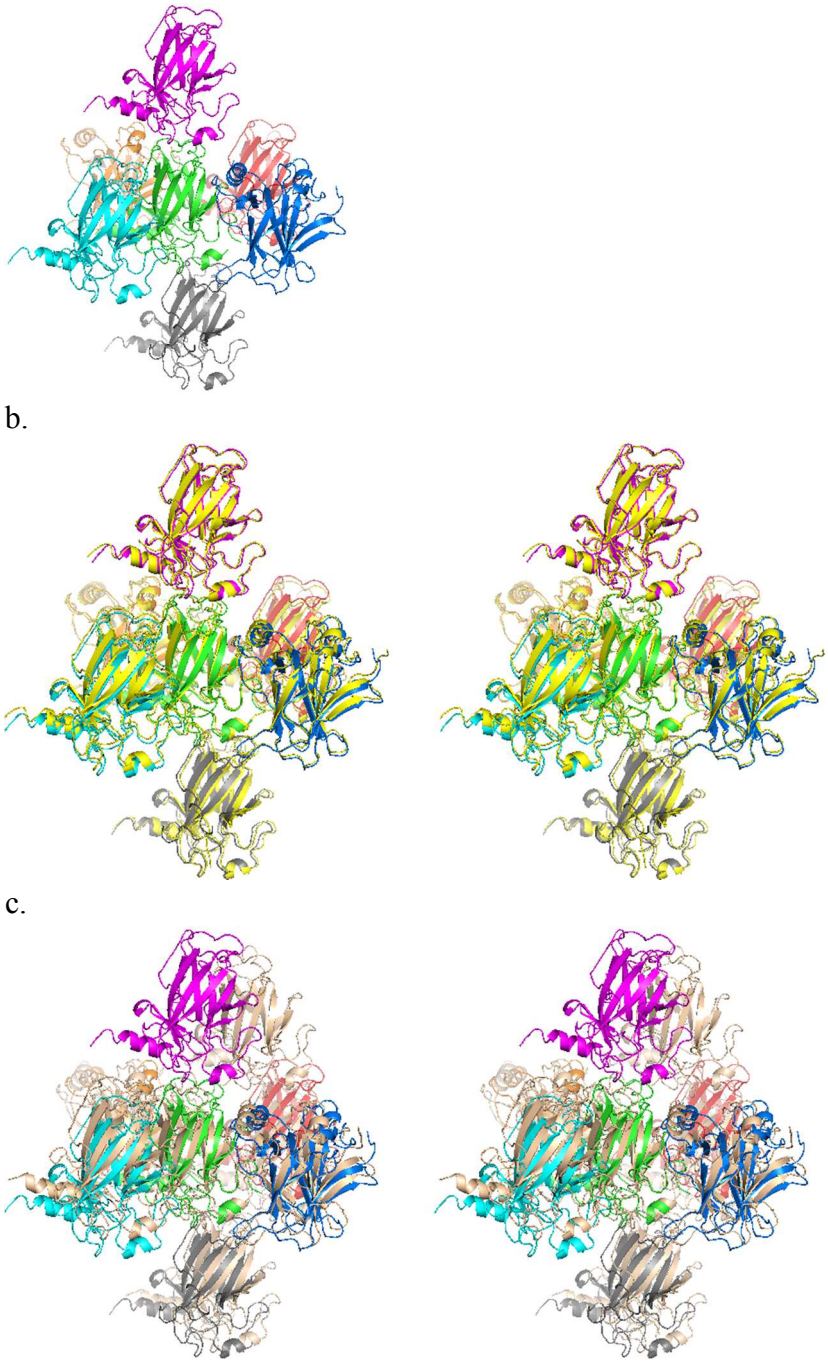

Figure 4.7. **Unit Cell of R248K (monomers) and Structural alignments with R248S and R248Q unit cells (monomers).** The unit cell of R248K monomers were constructed using Pymol (DeLano 2004) and aligned with two R248 mutants (Lefever 2014). (a) The unit cell R248K monomers were designated as follows: top (magenta), center (green), side 1 (cyan), side 2 (blue), side 3 (red), side 4 (orange), bottom (grey). (b) The R248K unit cell was superimposed with unit cell of R248S (yellow). (c). The stereoscopic image R248K unit cell was superimposed with unit cell of R248Q monomers.

Table 4.6. **R248K contacts within Unit Cell.** Within the R248K unit cell in Figure 4.7a, contacts were determined for each monomer in respect to the center monomer and categorized into Van der Waals, hydrogen bonding, or salt bridge interactions.

a.

	Center Monomer	**Top Monomer**
Van der Waals	Ser 106	Ala 276
	Tyr 107	Ala 276
	Asp 148	Arg 280
	Ser 149	Cys 277
	Ser 261	His 178
Hydrogen Bonding	Asp 148	Arg 280
	Ser 149	Arg 280
Salt Bridges	Asp 148	Arg 280

b.

	Center Monomer	**Side 1 Monomer**
Van der Waals	Ser 95	Gly 199
	Ser 95	Leu 201
	Lys 101	Ser 227
	Tyr 103	Val 225
Hydrogen Bonding	Ser 99	Glu 224
Salt Bridges	None	None

Table 4.6. (continued)

c.

	Center Monomer	Side 2 Monomer
Van der Waals	Arg 110	Arg 110
	Arg 110	Asp 148
	His 115	Pro 190
	His 115	Gln 192
	His 115	Asp 207
	Ser 116	Leu 206
	Gly 117	Glu 204
	Thr 118	Glu 204
	Pro 128	Gly 187
	Pro 128	Leu 188
	Ala 129	Leu 188
	Arg 283	Arg 156
	Glu 286	Arg 202
	Glu 287	Arg 202
	Leu 289	Leu 201
	Arg 290	Arg 202
Hydrogen Bonding	Arg 110	Arg 110
	Arg 110	Asp 148
	His 115	Asp 207
	Thr 118	Glu 204
	Arg 283	Arg 156
	Arg 283	Ser 260
Salt Bridges	Arg 110	Asp 148
	His 115	Asp 207

d.

	Center Monomer	Side 3 Monomer
Van der Waals	Leu 188	Phe 94
	Glu 198	Ser 166
	Glu 198	Gln 167
	Gly 199	Ser 166
	Gly 199	Met 169
	Leu 201	Ser 95
	Leu 201	Val 97
	Leu 201	Thr 170
Hydrogen Bonding	Glu 198	Gln 167
Salt Bridges	None	None

Table 4.6. (continued)

e.

	Center Monomer	Side 4 Monomer
	Arg 110	Arg 110
	Arg 110	Asp 148
	Arg 156	Arg 283
	Gly 187	Pro 128
	Leu 188	Pro 128
	Leu 188	Ala 129
	Pro 190	His 115
	Gln 192	His 115
	Leu 201	Leu 289
	Arg 202	Glu 286
	Arg 202	Glu 287
	Arg 202	Arg 290
	Glu 204	Gly 117
	Glu 204	Thr 118
	Leu 206	His 115
	Leu 206	Ser 116
Van der Waals	Asp 207	His 115
	Ser 260	Arg 283
	Arg 110	Arg 110
	Arg 110	Asp 148
	Arg 156	Arg 283
	Asp 184	Arg 110
	Glu 204	Thr 118
Hydrogen Bonding	Asp 207	His 115
	Ser 260	Arg 283
	Arg 110	Asp 148
Salt Bridges	Asp 184	Arg 110
	Asp 207	His 115

f.

	Center Monomer	Bottom Monomer
	His 178	Tyr 103
	His 178	Tyr 107
	His 178	Pro 152
	His 178	Asp 259
	His 178	Asn 263
	His 178	Leu 265
	His 179	Ser 106
	Arg 181	Asp 259
	Arg 181	Ser 260
	Arg 181	Ser 261
	Asn 239	Ser 106
	Ser 241	Tyr 103
	Cys 242	Tyr 103
Van der Waals	Cys 242	Ser 106
	Met 243	Tyr 103
	His 178	Tyr 107
	His 178	Asp 259
	Arg 181	Ser 260
	Arg 181	Ser 261
Hydrogen Bonding	Asn 239	Ser 106
	Met 243	Tyr 103
Salt Bridges	His 178	Asp 259

Table 4.7. **Comparison of Contacts between R248K unit cell (monomer) and R248S unit cell (monomer)**. Categorized contacts from each monomeric pair between R248K and R248S unit cell, shown in Table 4.6 and 4.2 respectively, were analyzed. Within each type of interaction, the total unique contacts amongst the two unit cells were divided into the following: same contacts, relative contacts, or different contacts. The number of contact pairs and percentage were shown for each respective criteria.
a.

Center Monomer - Top Monomer			
	Alignment Criteria	**Number of Contacts**	**% of Contacts**
	Same Contacts Pairs	0	0
	Relative Contact	0	0
Van der Waals	Different Contact Pairs	5	100.00
	Total	**5**	**100.00**
	Alignment Criteria	**Number of Contacts**	**% of Contacts**
	Same Contacts Pairs	0	0
Hydrogen	Relative Contact	3	100.00
Bonding	Different Contact Pairs	0	0
	Total	**3**	**100.00**
	Alignment Criteria	**Number of Contacts**	**% of Contacts**
	Same Contacts Pairs	0	0
	Relative Contact	0	0
Salt Bridges	Different Contact Pairs	1	100.00
	Total	**1**	**100.00**

Table 4.7. (continued)
b.

Center Monomer - Side 1 Monomer			
	Alignment Criteria	**Number of Contacts**	**% of Contacts**
Van der Waals	Same Contacts Pairs	2	33.33
	Relative Contact	0	0
	Different Contact Pairs	4	66.67
	Total	**6**	**100.00**
	Alignment Criteria	**Number of Contacts**	**% of Contacts**
Hydrogen Bonding	Same Contacts Pairs	0	0
	Relative Contact	2	100.00
	Different Contact Pairs	0	0
	Total	**2**	**100.00**
	Alignment Criteria	**Number of Contacts**	**% of Contacts**
Salt Bridges	Same Contacts Pairs	0	0
	Relative Contact	0	0
	Different Contact Pairs	1	**100.00**
	Total	**1**	**100.00**

c.

Center Monomer - Side 2 Monomer			
	Alignment Criteria	**Number of Contacts**	**% of Contacts**
Van der Waals	Same Contacts Pairs	11	61.11
	Relative Contact	4	22.22
	Different Contact Pairs	3	16.67
	Total	**6**	**100.00**
	Alignment Criteria	**Number of Contacts**	**% of Contacts**
Hydrogen Bonding	Same Contacts Pairs	4	44.44
	Relative Contact	1	11.11
	Different Contact Pairs	4	44.44
	Total	**9**	99.99
	Alignment Criteria	**Number of Contacts**	**% of Contacts**
Salt Bridges	Same Contacts Pairs	1	25.00
	Relative Contact	0	0
	Different Contact Pairs	3	75.00
	Total	**4**	**100.00**

Table 4.7. (continued)
d.

Center Monomer - Side 3 Monomer			
	Alignment Criteria	**Number of Contacts**	**% of Contacts**
	Same Contacts Pairs	0	0
	Relative Contact	0	0
Van der Waals	Different Contact Pairs	11	100.00
	Total	**11**	**100.00**
	Alignment Criteria	**Number of Contacts**	**% of Contacts**
	Same Contacts Pairs	0	0
Hydrogen	Relative Contact	0	0
Bonding	Different Contact Pairs	1	100.00
	Total	**1**	100.00
	Alignment Criteria	**Number of Contacts**	**% of Contacts**
	Same Contacts Pairs	0	0
	Relative Contact	0	0
Salt Bridges	Different Contact Pairs	0	0
	Total	**0**	**0**

e.

Center Monomer - Side 4 Monomer			
	Alignment Criteria	**Number of Contacts**	**% of Contacts**
	Same Contacts Pairs	13	72.22
	Relative Contact	3	16.67
Van der Waals	Different Contact Pairs	2	11.11
	Total	**18**	**100.00**
	Alignment Criteria	**Number of Contacts**	**% of Contacts**
	Same Contacts Pairs	4	44.44
	Relative Contact	1	11.11
Hydrogen Bonding	Different Contact Pairs	4	44.44
	Total	**9**	99.99
	Alignment Criteria	**Number of Contacts**	**% of Contacts**
	Same Contacts Pairs	1	33.33
	Relative Contact	0	0
Salt Bridges	Different Contact Pairs	2	66.67
	Total	**3**	**100.00**

Table 4.7 (continued)
f.

Center Monomer – Bottom Monomer			
	Alignment Criteria	**Number of Contacts**	**% of Contacts**
Van der Waals	Same Contacts Pairs	10	62.50
	Relative Contact	6	37.50
	Different Contact Pairs	0	0
	Total	**16**	**100.00**
	Alignment Criteria	**Number of Contacts**	**% of Contacts**
Hydrogen Bonding	Same Contacts Pairs	3	50.00
	Relative Contact	0	0
	Different Contact Pairs	3	50.00
	Total	**9**	100.00
	Alignment Criteria	**6**	**% of Contacts**
Salt Bridges	Same Contacts Pairs	1	100.00
	Relative Contact	0	0
	Different Contact Pairs	0	0
	Total	**3**	**100.00**

Table 4.8. **Comparison of Contacts between R248K unit cell (monomer) and R248Q unit cell (monomer)**. Within each type of interaction, total unique contacts from each monomeric pair between R248K and R248Q unit cell, shown in Table 4.6 and 4.1 respectively, were categorized into the following criteria: same contacts, relative contacts, or different contacts. The number of contact pairs and percentage were shown for each respective criteria.

a.

Center Monomer - Top Monomer			
	Alignment Criteria	**Number of Contacts**	**% of Contacts**
Van der Waals	Same Contacts Pairs	0	0
	Relative Contact	0	0
	Different Contact Pairs	7	100.00
	Total	**7**	**100.00**
	Alignment Criteria	**Number of Contacts**	**% of Contacts**
Hydrogen Bonding	Same Contacts Pairs	0	0
	Relative Contact	0	0
	Different Contact Pairs	4	100.00
	Total	**4**	100.00
	Alignment Criteria	**Number of Contacts**	**% of Contacts**
Salt Bridges	Same Contacts Pairs	0	0
	Relative Contact	0	0
	Different Contact Pairs	1	100.00
	Total	**1**	**100.00**

Table 4.8. (continued)
b.

Center Monomer - Side 1 Monomer			
	Alignment Criteria	**Number of Contacts**	**% of Contacts**
	Same Contacts Pairs	0	0
	Relative Contact	2	33.33
Van der Waals	Different Contact Pairs	4	66.67
	Total	**6**	**100.00**
	Alignment Criteria	**Number of Contacts**	**% of Contacts**
	Same Contacts Pairs	0	0
Hydrogen	Relative Contact	2	66.67
Bonding	Different Contact Pairs	1	33.33
	Total	**3**	100.00
	Alignment Criteria	**Number of Contacts**	**% of Contacts**
	Same Contacts Pairs	0	0
	Relative Contact	0	0
Salt Bridges	Different Contact Pairs	0	0
	Total	**0**	**0**

c.

Center Monomer - Side 2 Monomer			
	Alignment Criteria	**Number of Contacts**	**% of Contacts**
	Same Contacts Pairs	11	55.00
	Relative Contact	2	10.00
Van der Waals	Different Contact Pairs	7	35.00
	Total	**20**	**100.00**
	Alignment Criteria	**Number of Contacts**	**% of Contacts**
	Same Contacts Pairs	4	57.14
Hydrogen	Relative Contact	0	0
Bonding	Different Contact Pairs	3	42.86
	Total	**7**	100.00
	Alignment Criteria	**Number of Contacts**	**% of Contacts**
	Same Contacts Pairs	1	33.33
	Relative Contact	0	0
Salt Bridges	Different Contact Pairs	2	66.67
	Total	**3**	**100.00**

Table 4.8. (continued)
d.

Center Monomer - Side 3 Monomer			
	Alignment Criteria	**Number of Contacts**	**% of Contacts**
Van der Waals	Same Contacts Pairs	0	0
	Relative Contact	4	26.67
	Different Contact Pairs	11	73.33
	Total	**15**	**100.00**
	Alignment Criteria	**Number of Contacts**	**% of Contacts**
Hydrogen Bonding	Same Contacts Pairs	0	0
	Relative Contact	0	0
	Different Contact Pairs	3	100.00
	Total	**3**	100.00
	Alignment Criteria	**Number of Contacts**	**% of Contacts**
Salt Bridges	Same Contacts Pairs	0	0
	Relative Contact	0	0
	Different Contact Pairs	0	0
	Total	**0**	**0**

e.

Center Monomer - Side 4 Monomer			
	Alignment Criteria	**Number of Contacts**	**% of Contacts**
Van der Waals	Same Contacts Pairs	12	57.14
	Relative Contact	0	0
	Different Contact Pairs	9	42.86
	Total	**21**	**100.00**
	Alignment Criteria	**Number of Contacts**	**% of Contacts**
Hydrogen Bonding	Same Contacts Pairs	4	50.00
	Relative Contact	0	0
	Different Contact Pairs	4	50.00
	Total	**8**	**100.00**
	Alignment Criteria	**Number of Contacts**	**% of Contacts**
Salt Bridges	Same Contacts Pairs	1	33.33
	Relative Contact	0	0
	Different Contact Pairs	2	66.67
	Total	**3**	**100.00**

Table 4.8. (continued)
f.

Center Monomer - Bottom Monomer			
	Alignment Criteria	**Number of Contacts**	**% of Contacts**
Van der Waals	Same Contacts Pairs	11	45.83
	Relative Contact	9	37.50
	Different Contact Pairs	4	16.67
	Total	**24**	**100.00**
	Alignment Criteria	**Number of Contacts**	**% of Contacts**
Hydrogen Bonding	Same Contacts Pairs	3	30.00
	Relative Contact	3	30.00
	Different Contact Pairs	4	40.00
	Total	**10**	**100.00**
	Alignment Criteria	**Number of Contacts**	**% of Contacts**
Salt Bridges	Same Contacts Pairs	1	50.00
	Relative Contact	1	50.00
	Different Contact Pairs	0	0
	Total	**2**	**100.00**

Table 4.9. **Data collection statistics of Y103K p53 DBD**. The data collection statistics of Y103K p53 DBDwas determined using Mosflm (Leslie and Powell 2007).

Data Collection	Y103K p53DBD
Beamline	SSRL
Wavelength (□)	1.127
Space group	1 21 1
Cell dimensions	
a, b, c (□)	44.32, 68.45, 64.29
α = γ (°)	90
β (°)	101.08
Resolution (□)	50-1.850
Rsym or Rmerge	0.082
I/σI	15.1 (11.6)
Completeness (%)	99.9 (100.0)
Redundancy	3.7 (3.6)

Table 4.10. **Refinement statistics of Y103K p53 DBD**. Refinement statistics of Y103K p53 DBD was determined using PHENIX (Adams et al 2010), Coot 0.7 (Adams et al 2010), PROCHECK (Laskowski et al 1993).

Refinement statistics	Y103K p53DBD
Refinement	
Resolution (Å)	43.494 - 1.850
No. reflections	32113
Rwork/Rfree	18.43/20.71
Molecules in A.U.	2
No. atoms	3539
Protein	3168
Zn^{2+} ion	2
Water	371
B-factors	21.1
Protein	20.52
Zn^{2+} ion	15
Water	26.367
R.m.s. deviations	
Bond lengths (Å)	0.008
Bond angles (°)	1.086
Dihedral angles (°)	12.53
Ramachandran Plot	
Most favored region	90.3
Additionally allowed region	9.7
Generously allowed region	0
Disallowed region	0

a.

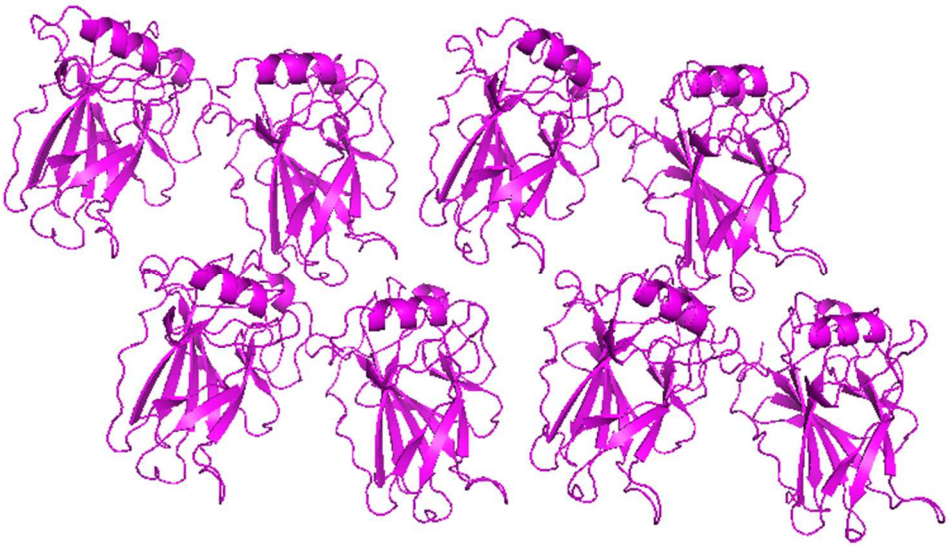

b.

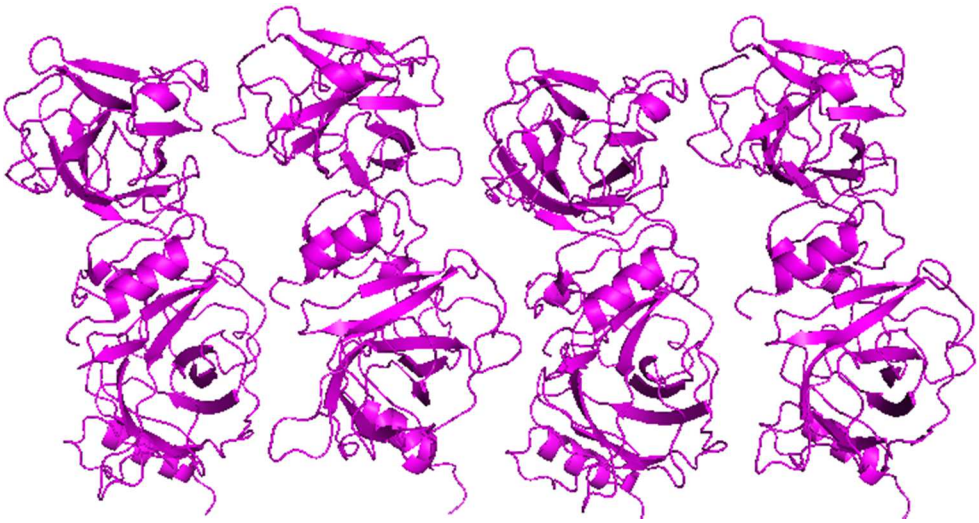

Figure 4.8. **Unit Cell of Y103K p53 DBD mutant**. The unit cell of dimeric Y103K p53 DBD mutant was constructed using Pymol (DeLano 2004). The unit cell was generated with symmetry mates at one unit cell within 4 Å. (a) Unit cell of Y103K p53 DBD in the x-y plane. (b) Unit cell of Y103K p53 DBD in the z-x plane.

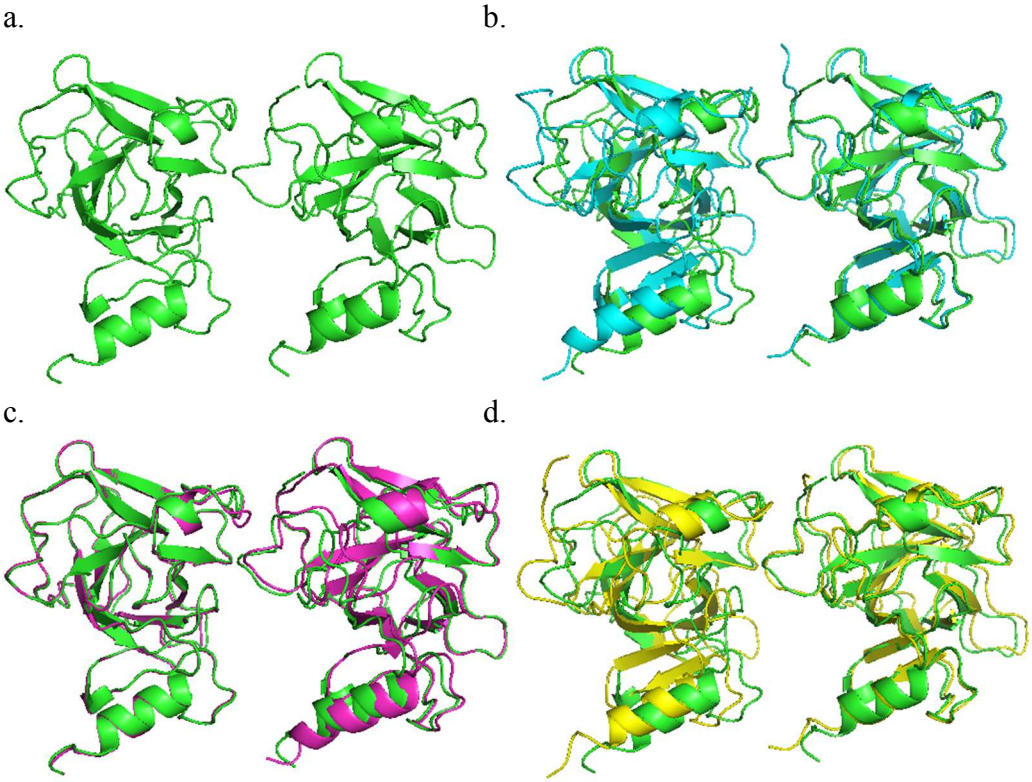

Figure 4.9. **Structural Alignment of Dimeric Mutant Y103K p53 DBD with three R248 p53 DBD mutants.** The dimer of mutant Y103K p53 DBD was constructed using Pymol (DeLano 2004), which was superimposed with three R248 p53 DBD mutants. (a) Dimeric Y103K p53 DBD. (b) Alignment of dimeric Y103K p53 DBD (green) with dimeric R248K p53 DBD (blue). (c) Alignment of Y103K p53 DBD (green) with R248Q p53 DBD (magenta). (d) Alignment of Y103K p53 DBD (green) with R248S p53 DBD (yellow).

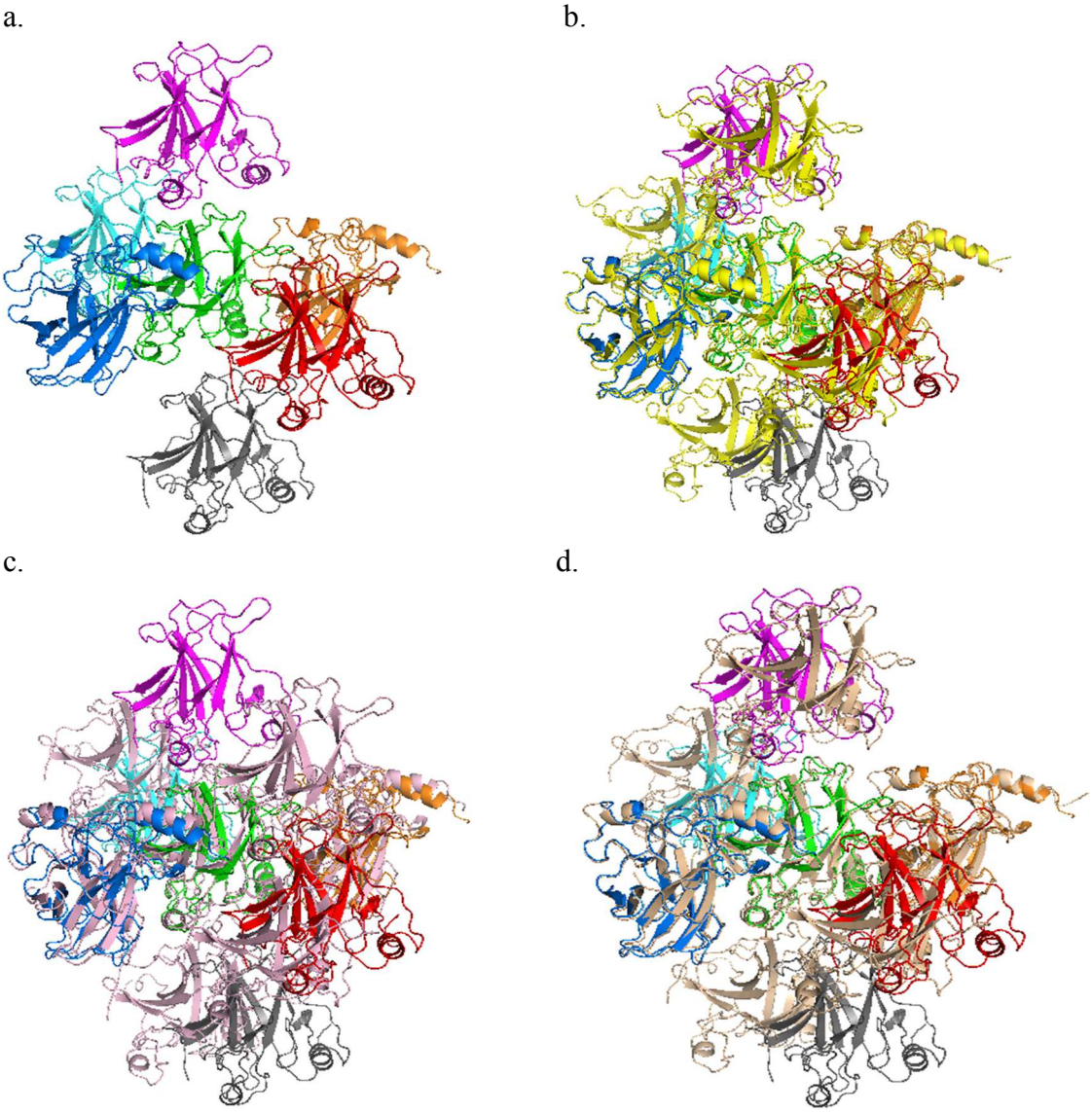

Figure 4.10. **Unit Cell of Y103K (monomers) and Structural alignments with R248 mutant monomeric unit cells.** The unit cell of Y103K monomers were constructed using Pymol (DeLano 2004) and aligned with three mutant R248 unit cells. The unit cell consisted of monomers instead of dimers for the ease of visualization. (a) The Y103K monomers within the unit cell were designated by the following colors: magenta (top), center (green), side 1 (cyan), side 2 (blue), side 3 (red), side 4 (orange), bottom (grey). (b) The Y103K unit cell in Figure 4.10a was superimposed with unit cell of R248K monomers (yellow). (c) The Y103K unit cell in Figure 4.10a was superimposed with unit cell of R248Q monomers (light pink). (d) The Y103K unit cell in Figure 4.10a was superimposed with unit cell of R248S monomers (beige).

Table 4.11. **Y103K contacts within Unit Cell.** Within the R248K unit cell in Figure 4.10a, contacts were determined for each monomer in respect to the center monomer and categorized into Van der Waals, hydrogen bonding, or salt bridge interactions.

a.

	Center Monomer	**Top Monomer**
Van der Waals	Lys 103	Met 243
	Lys 103	Asn 247
	Gly 105	Ser 241
	Ser 106	His 179
	Ser 106	Ser 241
	Ser 106	Cys 242
	Tyr 107	His 178
	Pro 152	His 178
	Asp 259	His 178
	Asn 263	His 178
	Asn 263	Pro 177
	Asn 263	His 178
	Leu 264	Met 243
	Leu 265	His 178
	Leu 265	Met 243
	Gly 266	Met 243
	Arg 267	Met 243
Hydrogen Bonding	Ser 106	Asn 239
	Gly 105	Ser 241
	Ser 106	Asn 239
	Tyr 107	His 178
	Lys 103	Asn 247
Salt Bridges	None	None

b.

	Center Monomer	**Side 1 Monomer**
Van der Waals	Phe 94	Ser 183
	Ser 166	Ala 138
	Gln 167	Ala 138
	Gln 167	Leu 137
	Gln 167	Ala 138
	Gln 167	Asp 184
	Gln 167	Met 237
	Thr 170	Gly 185
	Thr 170	Asp 186
Hydrogen Bonding	Thr 170	Gly 185
Salt Bridges	None	None

Table 4.11. (continued)

c.

	Center Monomer	Side 2 Monomer
Van der Waals	Arg 156	Arg 283
	Leu 188	Ala 129
	Leu 188	Pro 128
	Pro 190	His 115
	Gly 199	Thr 118
	Gly 199	Lys 291
	Asn 200	Lys 291
	Leu 201	Leu 289
	Leu 201	Arg 290
	Leu 201	Lys 291
	Arg 202	Glu 286
	Arg 202	Glu 287
	Glu 204	Gly 117
	Glu 204	Thr 118
	Glu 204	Arg 282
	Leu 206	His 115
	Leu 206	Ser 116
	Leu 206	Gly 117
	Asp 207	Glu 204
	Asp 207	His 115
	Ser 260	Arg 283
Hydrogen Bonding	Arg 156	Thr 118
	Arg 156	Arg 283
	Leu 201	Lys 291
	Glu 204	Thr 118
	Asp 207	His 115
	Glu 221	Lys 291
	Ser 260	Arg 283
Salt Bridges	Asp 207	His 115
	Glu 221	Lys 291

d.

	Center monomer	Side 3 monomer
Van der Waals	Glu 224	Lys 103
	Glu 224	Ser 106
	Val 225	Ser 106
Hydrogen Bonding	Glu 224	Lys 103
	Val 225	Ser 106
Salt Bridges	Glu 224	Lys 103

Table 4.11. (continued)

e.

	Center monomer	Side 4 monomer
Van der Waals	His 115	Pro 190
	His 115	Leu 201
	His 115	Leu 206
	His 115	Asp 207
	Ser 116	Leu 206
	Gly 117	Glu 204
	Gly 117	Leu 206
	Thr 118	Glu 204
	Pro 128	Leu 188
	Ala 129	Leu 188
	Arg 282	Glu 204
	Arg 283	Arg 156
	Arg 283	Ser 260
	Glu 286	Arg 202
	Glu 287	Arg 202
	Leu 289	Leu 201
	Arg 290	Leu 201
	Lys 291	Gly 199
	Lys 291	Asn 200
	Lys 291	Leu 201
Hydrogen Bonding	His 115	Asp 207
	Thr 118	Arg 156
	Thr 118	Glu 204
	Thr 118	Glu 221
	Arg 283	Arg 156
	Arg 283	Ser 260
	Lys 291	Glu 221
Salt Bridges	His 115	Asp 207
	Lys 291	Glu 221

f.

	Center monomer	Bottom monomer
Van der Waals	Lys 120	Asp 148
	Cys 277	Ser 149
Hydrogen Bonding	Lys 120	Asp 148
Salt Bridges	Lys 120	Asp 148

Table 4.12. **Comparison of Contacts between Y103K unit cell (monomer) and R248K unit cell (monomer)**. Categorized contacts from each monomeric pair between Y103K and R248K unit cell, shown in Table 4.11 and 4.6 respectively, were analyzed. Within each type of interaction, the total unique contacts amongst the two unit cells were divided into the following: same contacts, relative contacts, or different contacts. The number of contact pairs and percentage were shown for each respective criteria.
a.

Center Monomer - Top Monomer			
	Alignment Criteria	**Number of Contacts**	**% of Contacts**
Van der Waals	Same Contacts Pairs	0	0.00%
	Relative Contact	8	36.36%
	Different Contact Pairs	14	63.64%
	Total	**22**	**100.00%**
	Alignment Criteria	**Number of Contacts**	**% of Contacts**
Hydrogen Bonding	Same Contacts Pairs	0	0.00%
	Relative Contact	0	0.00%
	Different Contact Pairs	6	100.00%
	Total	**6**	**100.00%**
	Alignment Criteria	**Number of Contacts**	**% of Contacts**
Salt Bridges	Same Contacts Pairs	0	0.00%
	Relative Contact	0	0.00%
	Different Contact Pairs	1	100.00%
	Total	**1**	**100.00%**

Table 4.12. (continued)
b.

Center Monomer - Side 1 Monomer			
	Alignment Criteria	**Number of Contacts**	**% of Contacts**
Van der Waals	Same Contacts Pairs	0	0.00
	Relative Contact	0	0.00
	Different Contact Pairs	13	100.00
	Total	**13**	**100.00**
	Alignment Criteria	**Number of Contacts**	**% of Contacts**
Hydrogen Bonding	Same Contacts Pairs	0	0.00
	Relative Contact	0	0.00
	Different Contact Pairs	2	100.00
	Total	**2**	**100.00**
	Alignment Criteria	**Number of Contacts**	**% of Contacts**
Salt Bridges	Same Contacts Pairs	0	0.00
	Relative Contact	0	0.00
	Different Contact Pairs	0	0.00
	Total	**0**	**0.00**

c.

Center Monomer - Side 2 Monomer			
	Alignment Criteria	**Number of Contacts**	**% of Contacts**
Van der Waals	Same Contacts Pairs	11	50.00
	Relative Contact	5	22.73
	Different Contact Pairs	6	27.27
	Total	**22**	**100.00**
	Alignment Criteria	**Number of Contacts**	**% of Contacts**
Hydrogen Bonding	Same Contacts Pairs	4	44.44
	Relative Contact	0	0.00
	Different Contact Pairs	5	55.56
	Total	**9**	**100.00**
	Alignment Criteria	**Number of Contacts**	**% of Contacts**
Salt Bridges	Same Contacts Pairs	1	33.33
	Relative Contact	0	0.00
	Different Contact Pairs	2	66.67
	Total	**3**	**100.00**

Table 4.12. (continued)
d.

Center Monomer - Side 3 Monomer			
	Alignment Criteria	**Number of Contacts**	**% of Contacts**
Van der Waals	Same Contacts Pairs	0	0.00
	Relative Contact	0	0.00
	Different Contact Pairs	11	100.00
	Total	**11**	**100.00**
	Alignment Criteria	**Number of Contacts**	**% of Contacts**
Hydrogen Bonding	Same Contacts Pairs	0	0.00
	Relative Contact	0	0.00
	Different Contact Pairs	3	100.00
	Total	**3**	**100.00**
	Alignment Criteria	**Number of Contacts**	**% of Contacts**
Salt Bridges	Same Contacts Pairs	0	0.00
	Relative Contact	0	0.00
	Different Contact Pairs	1	100.00
	Total	**1**	**100.00**

e.

Center Monomer - Side 4 Monomer			
	Alignment Criteria	**Number of Contacts**	**% of Contacts**
Van der Waals	Same Contacts Pairs	13	59.09
	Relative Contact	6	27.27
	Different Contact Pairs	3	13.64
	Total	**22**	**100.00**
	Alignment Criteria	**Number of Contacts**	**% of Contacts**
Hydrogen Bonding	Same Contacts Pairs	4	40.00
	Relative Contact	2	20.00
	Different Contact Pairs	4	40.00
	Total	**10**	**100.00**
	Alignment Criteria	**Number of Contacts**	**% of Contacts**
Salt Bridges	Same Contacts Pairs	1	25.00
	Relative Contact	0	0.00
	Different Contact Pairs	3	75.00
	Total	**4**	**100.00**

Table 4.12. (continued)
f.

Center Monomer - Bottom Monomer			
	Alignment Criteria	**Number of Contacts**	**% of Contacts**
Van der Waals	Same Contacts Pairs	0	0.00
	Relative Contact	0	0.00
	Different Contact Pairs	17	100.00
	Total	**17**	**100.00**
	Alignment Criteria	**Number of Contacts**	**% of Contacts**
Hydrogen Bonding	Same Contacts Pairs	0	0.00
	Relative Contact	0	0.00
	Different Contact Pairs	7	100.00
	Total	**7**	**100.00**
	Alignment Criteria	**Number of Contacts**	**% of Contacts**
Salt Bridges	Same Contacts Pairs	0	0.00
	Relative Contact	0	0.00
	Different Contact Pairs	2	100.00
	Total	**2**	**100.00**

Table 4.13. **Comparison of Contacts between Y103K unit cell (monomer) and R248Q unit cell (monomer)**. Categorized contacts from each monomeric pair between Y103K and R248Q unit cell, shown in Table 4.11 and 4.1 respectively, were analyzed. Within each type of interaction, the total unique contacts amongst the two unit cells were divided into the following: same contacts, relative contacts, or different contacts. The number of contact pairs and percentage were shown for each respective criteria.

a.

Center Monomer - Top Monomer			
	Alignment Criteria	**Number of Contacts**	**% of Contacts**
Van der Waals	Same Contacts Pairs	0	0.00
	Relative Contact	0	0.00
	Different Contact Pairs	19	100.00
	Total	**19**	**100.00**
	Alignment Criteria	**Number of Contacts**	**% of Contacts**
Hydrogen Bonding	Same Contacts Pairs	0	0.00
	Relative Contact	0	0.00
	Different Contact Pairs	6	100.00
	Total	**6**	**100.00**
	Alignment Criteria	**Number of Contacts**	**% of Contacts**
Salt Bridges	Same Contacts Pairs	0	0.00
	Relative Contact	0	0.00
	Different Contact Pairs	0	0.00
	Total	**0**	**0.00**

Table 4.13. (continued)
b.

Center Monomer - Side 1 Monomer			
	Alignment Criteria	**Number of Contacts**	**% of Contacts**
Van der Waals	Same Contacts Pairs	0	0.00
	Relative Contact	0	0.00
	Different Contact Pairs	13	100.00
	Total	**13**	**100.00**
	Alignment Criteria	**Number of Contacts**	**% of Contacts**
Hydrogen Bonding	Same Contacts Pairs	0	0.00
	Relative Contact	0	0.00
	Different Contact Pairs	3	100.00
	Total	**3**	**100.00**
	Alignment Criteria	**Number of Contacts**	**% of Contacts**
Salt Bridges	Same Contacts Pairs	0	0.00
	Relative Contact	0	0.00
	Different Contact Pairs	0	0.00
	Total	**0**	**0.00**

c.

Center Monomer - Side 2 Monomer			
	Alignment Criteria	**Number of Contacts**	**% of Contacts**
Van der Waals	Same Contacts Pairs	14	66.67
	Relative Contact	2	9.52
	Different Contact Pairs	5	23.81
	Total	**21**	**100.00**
	Alignment Criteria	**Number of Contacts**	**% of Contacts**
Hydrogen Bonding	Same Contacts Pairs	5	71.43
	Relative Contact	2	28.57
	Different Contact Pairs	0	0.00
	Total	**7**	**100.00**
	Alignment Criteria	**Number of Contacts**	**% of Contacts**
Salt Bridges	Same Contacts Pairs	2	100.00
	Relative Contact	0	0.00
	Different Contact Pairs	0	0.00
	Total	**2**	**100.00**

Table 4.13. (continued)
d.

Center Monomer - Side 3 Monomer			
	Alignment Criteria	**Number of Contacts**	**% of Contacts**
Van der Waals	Same Contacts Pairs	0	0.00
	Relative Contact	0	0.00
	Different Contact Pairs	10	100.00
	Total	**10**	**100.00%**
	Alignment Criteria	**Number of Contacts**	**% of Contacts**
Hydrogen Bonding	Same Contacts Pairs	0	0.00
	Relative Contact	0	0.00
	Different Contact Pairs	4	100.00
	Total	**4**	**100.00**
	Alignment Criteria	**Number of Contacts**	**% of Contacts**
Salt Bridges	Same Contacts Pairs	0	0.00
	Relative Contact	0	0.00
	Different Contact Pairs	1	100.00
	Total	**1**	**100.00**

e.

Center Monomer - Side 4 Monomer			
	Alignment Criteria	**Number of Contacts**	**% of Contacts**
Van der Waals	Same Contacts Pairs	14	66.67
	Relative Contact	6	28.57
	Different Contact Pairs	1	4.76
	Total	**21**	**100.00**
	Alignment Criteria	**Number of Contacts**	**% of Contacts**
Hydrogen Bonding	Same Contacts Pairs	4	50.00
	Relative Contact	4	50.00
	Different Contact Pairs	0	0.00
	Total	**8**	**100.00**
	Alignment Criteria	**Number of Contacts**	**% of Contacts**
Salt Bridges	Same Contacts Pairs	1	50.00
	Relative Contact	0	0.00
	Different Contact Pairs	1	50.00
	Total	**2**	**100.00**

Table 4.13. (continued)
f.

Center Monomer - Bottom Monomer			
	Alignment Criteria	**Number of Contacts**	**% of Contacts**
Van der Waals	Same Contacts Pairs	0	0.00
	Relative Contact	0	0.00
	Different Contact Pairs	21	100.00
	Total	**21**	**100.00**
	Alignment Criteria	**Number of Contacts**	**% of Contacts**
Hydrogen Bonding	Same Contacts Pairs	0	0.00
	Relative Contact	0	0.00
	Different Contact Pairs	8	100.00
	Total	**8**	**100.00**
	Alignment Criteria	**Number of Contacts**	**% of Contacts**
Salt Bridges	Same Contacts Pairs	0	0.00
	Relative Contact	0	0.00
	Different Contact Pairs	3	100.00
	Total	**3**	**100.00**

Table 4.14. **Comparison of Contacts between Y103K unit cell (monomer) and R248S unit cell (monomer)**. Categorized contacts from each monomeric pair between R248K and R248S unit cell, shown in Table 4.11 and 4.2 respectively, were analyzed. Within each type of interaction, the total unique contacts amongst the two unit cells were divided into the following: same contacts, relative contacts, or different contacts. The number of contact pairs and percentage were shown for each respective criteria.
a.

Center Monomer - Top Monomer			
	Alignment Criteria	**Number of Contacts**	**% of Contacts**
Van der Waals	Same Contacts Pairs	0	0.00
	Relative Contact	0	0.00
	Different Contact Pairs	17	100.00
	Total	**17**	**100.00**
	Alignment Criteria	**Number of Contacts**	**% of Contacts**
Hydrogen Bonding	Same Contacts Pairs	0	0.00
	Relative Contact	0	0.00
	Different Contact Pairs	5	100.00
	Total	**5**	**100.00**
	Alignment Criteria	**Number of Contacts**	**% of Contacts**
Salt Bridges	Same Contacts Pairs	0	0.00
	Relative Contact	0	0.00
	Different Contact Pairs	0	0.00
	Total	**0**	**0.00**

Table 4.14. (continued)
b.

Center Monomer - Side 1 Monomer			
	Alignment Criteria	**Number of Contacts**	**% of Contacts**
Van der Waals	Same Contacts Pairs	0	0.00
	Relative Contact	0	0.00
	Different Contact Pairs	9	100.00
	Total	**9**	**100.00**
	Alignment Criteria	**Number of Contacts**	**% of Contacts**
Hydrogen Bonding	Same Contacts Pairs	0	0.00
	Relative Contact	0	0.00
	Different Contact Pairs	2	100.00
	Total	**2**	**100.00**
	Alignment Criteria	**Number of Contacts**	**% of Contacts**
Salt Bridges	Same Contacts Pairs	0	0.00
	Relative Contact	0	0.00
	Different Contact Pairs	1	100.00
	Total	**1**	**100.00**

c.

Center Monomer - Side 2 Monomer			
	Alignment Criteria	**Number of Contacts**	**% of Contacts**
Van der Waals	Same Contacts Pairs	12	48.00
	Relative Contact	7	28.00
	Different Contact Pairs	6	24.00
	Total	**25**	**100.00%**
	Alignment Criteria	**Number of Contacts**	**% of Contacts**
Hydrogen Bonding	Same Contacts Pairs	5	55.56
	Relative Contact	0	0.00
	Different Contact Pairs	4	44.44
	Total	**9**	**100.00**
	Alignment Criteria	**Number of Contacts**	**% of Contacts**
Salt Bridges	Same Contacts Pairs	1	25.00
	Relative Contact	0	0.00
	Different Contact Pairs	3	75.0
	Total	**4**	**100.00**

Table 4.14. (continued)
d.

Center Monomer - Side 3 Monomer			
	Alignment Criteria	**Number of Contacts**	**% of Contacts**
Van der Waals	Same Contacts Pairs	0	0.00
	Relative Contact	0	0.00
	Different Contact Pairs	6	100.00
	Total	**6**	**100.00**
	Alignment Criteria	**Number of Contacts**	**% of Contacts**
Hydrogen Bonding	Same Contacts Pairs	0	0.00
	Relative Contact	0	0.00
	Different Contact Pairs	2	100.00
	Total	**2**	**100.00**
	Alignment Criteria	**Number of Contacts**	**% of Contacts**
Salt Bridges	Same Contacts Pairs	0	0.00
	Relative Contact	0	0.00
	Different Contact Pairs	1	100.00
	Total	**1**	**100.00**

e.

Center Monomer - Side 4 Monomer			
	Alignment Criteria	**Number of Contacts**	**% of Contacts**
Van der Waals	Same Contacts Pairs	11	57.89
	Relative Contact	5	26.32
	Different Contact Pairs	3	15.79
	Total	**19**	**100.00**
	Alignment Criteria	**Number of Contacts**	**% of Contacts**
Hydrogen Bonding	Same Contacts Pairs	5	62.50
	Relative Contact	1	12.50
	Different Contact Pairs	2	25.00
	Total	**8**	**100.00**
	Alignment Criteria	**Number of Contacts**	**% of Contacts**
Salt Bridges	Same Contacts Pairs	1	50.00
	Relative Contact	0	0.00
	Different Contact Pairs	1	50.00
	Total	**2**	**100.00**

Table 4.14. (continued)
f.

Center Monomer - Bottom Monomer			
	Alignment Criteria	**Number of Contacts**	**% of Contacts**
Van der Waals	Same Contacts Pairs	0	0.00
	Relative Contact	0	0.00
	Different Contact Pairs	13	100.00
	Total	**13**	**100.00**
	Alignment Criteria	**Number of Contacts**	**% of Contacts**
Hydrogen Bonding	Same Contacts Pairs	0	0.00
	Relative Contact	0	0.00
	Different Contact Pairs	4	100.00
	Total	**4**	**100.00**
	Alignment Criteria	**Number of Contacts**	**% of Contacts**
Salt Bridges	Same Contacts Pairs	0	0.00
	Relative Contact	0	0.00
	Different Contact Pairs	2	100.00
	Total	**2**	**100.00**

Chapter Five

In Search of Reversing Filament Formation by Mutations or Interaction with p73

5.1 Thioflavin T Fluorescence Assays of Mutants Y103A, Y103K and Y103E and Double Mutants R248Q/Y103A, R248Q/Y103K and R248Q/Y103E

The thioflavin T fluorescence assay was repeated with another set of mutant p53 DNA binding domain, as shown in Figure 5.1, consisting of single residue mutants and double mutants; the mutants with a single mutation at Y103 were treated as the control to compare against the mutant R248Q that had an additional mutation made in residue Y103. Each of the single residue mutant and double mutant exhibited the ability to form amyloid fibrils. The order from increasing rate of amyloid fibril formation consisted of the following p53 DBD proteins: wild-type, Y103A, Y103K, R248Q/Y103K, R248Q/Y103E, Y103E, R248Q/Y103A, and R248Q. This order corresponded to the thioflavin$_{(t1/2)}$ bound values present in Table 5.1. Examining the Th$_{(t1/2)}$ values indicated that the single residue mutants formed amyloid fibrils faster than their double mutant counterparts. In comparison to the Th$_{(t1/2)}$ bound value for R248Q, the addition of the second mutation in Y103 displayed lower Th$_{(t1/2)}$ bound values than the single mutant R248Q; the lower Th$_{(t1/2)}$ bound value indicated a shorter amount of time it took for the protein fraction to reach half bound to the ThT dye. This is also evident when comparing the Y103 mutants to wild-type p53 DBD, in which mutation made in Y103 displayed a lower Th$_{(t1/2)}$ bound value in comparison to the wild-type.

5.2 Amyloid Seeding of wild-type p73 DBD by Aggregated R248Q and Heterogeneous Thioflavin T Assay Involving R248Q p53DBD Mutant and Wild-type p73DBD

The amyloid seeding assay involving seeding mature mutant R248Q p53 DBD fibrils with soluble p73 DBD, the results revealed amyloid formation behavior differing from the wild-type. According to Figure 5.2 and Table 5.2, there was a significant onset of amyloid formation at 5 μM of p73 DBD, but at 10 μM p73 DBD there was only a slight increased in the rate of fibril formation compared to the control and delayed rate when comparing the results at 5 μM p73 DBD. Unlike the seeding assay in the presence of wild-type p53 DBD, the presence of p73 DBD at increased concentrations displayed a gradual decrease in rate of amyloid fibril formation compared to a less concentrated p73 DBD sample. The delayed rate of amyloid formation suggests the importance of complementarity between the growth face of the seed and the substrate; structural surface differences between p73 DBD and mutant R248Q suggest a key role in the ability for the fibril seed to inactivate its substrate, as well as the elongation and packing of the mature amyloid fibril.

The heterogeneous thioflavin T assay involved determining the rate of fibril formation for a mixture consisting of a soluble mutant R248Q p53 DBD and soluble wild-type p73 DBD; assay was repeated with the same concentration of mutant R248Q p53 DBD and varied concentrations of wild-type p73 DBD. Thioflavin T assay involving 5 μM mutant R248Q p53 DBD and 1 μM wild-type p73 DBD displayed similar rate of amyloid fibril formation as wild-type p73 DBD control, which was validated by the $Th_{(t1/2)}$ bound value in Table 5.3 and overlapping curves seen in Figure 5.3. By examining the curves shown in Figure 5.3 and $Th_{(t1/2)}$ bound values in Table 5.3, assays involving 5 μM and 10 μM wild-type p73 DBD had similar rate of fibril formation as mutant R248Q

p53 DBD. Assays using concentrations of 15 μM and 20 μM p73 DBD illustrated a gradual delay in fibril formation, deviating to the right from mixtures with 5 μM and 10 μM wild-type p73 DBD, as seen in Figure 5.3 and validated by $Th_{(t1/2)}$ bound values in Table 3.20. In addition, assays using concentrations of 15 μM and 20 μM p73 DBD formed fibrils faster than the p73 DBD control and the assay using 1 μM p73 DBD based on comparison to $Th_{(t1/2)}$ bound value in Table 5.3 and curves shown in Figure 5.3.

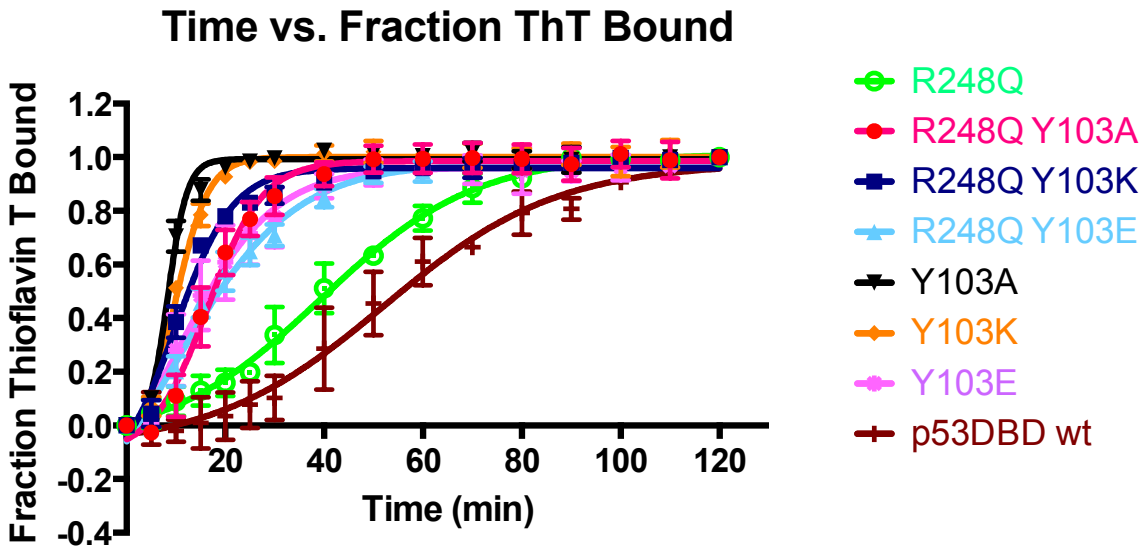

Figure 5.1. **Thioflavin T fluorescence Assay**. The thioflavin T assay was conducted using 5 µM protein and 25 µM thioflavin T, which was then incubated at 37ºC for 2 hours. The fluorescence intensity was measured at an excitation of 450 nm and emission of 480 nm, and the aggregation fraction was then calculated. Double mutants were compared to their corresponding single mutant.

Table 5.1. **Thioflavin$_{(t1/2)}$ Bound**. The thioflavin$_{(t1/2)}$ bound values, in minutes, were determined for each mutant and double mutant shown in Figure 3.9. The Th$_{(t1/2)}$ bound value represents the time it took for the sample to reach half of the fraction bound to Thioflavin T and half remaining in a folded state.

Mutant	ThT$_{1/2}$ Bound (min)
Y103A	8
Y103K	10
R248Q Y103K	10
R248Q Y103E	10
Y103E	11
R248Q Y103A	16
R248Q	39
wild-type p53DBD	52

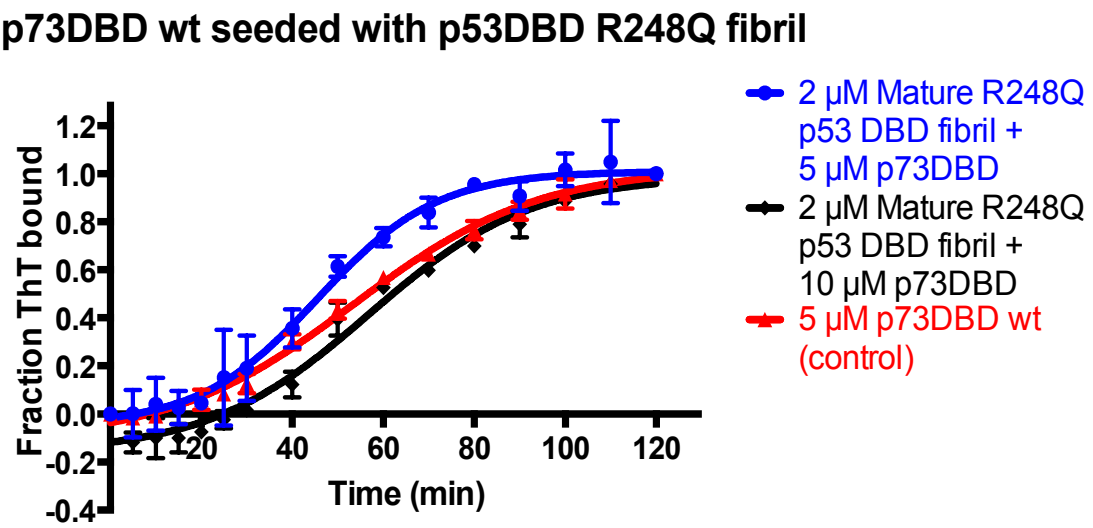

Figure 5.2. **Amyloid seeding assay of wild-type p73 DBD seeded with mutant R248Q p53DBD mature fibrils**. Sample of 20 µM mutant p53DBD R248Q was incubated at 37ºC for 30 minutes. R248Q fibrils were diluted to 2 µM in a sample containing 5 µM soluble p73DBD wt and 25 µM Thioflavin T. The mixture was then incubated at 37ºC for 2 hours. Fluorescence intensity was measured at excitation of 450 nm and emission of 480 nm; from the values, the aggregation fraction was calculated. Seeding assay was repeated using 10 µM soluble p73DBD wt. Wild-type p73DBD without the seeded mutant fibril was used as a control.

Table 5.2. **Thioflavin $_{(t1/2)}$ Bound for Amyloid Seeding Assay**. The Thioflavin $_{(t1/2)}$ bound values, in minutes, was determined for each of the seeded assay shown in Figure 5.2.

Mutant	$ThT_{1/2}$ Bound (min)
Seeded p73DBD (5 µM)	46
p73DBD wt	54
Seeded p73DBD (10 µM)	57

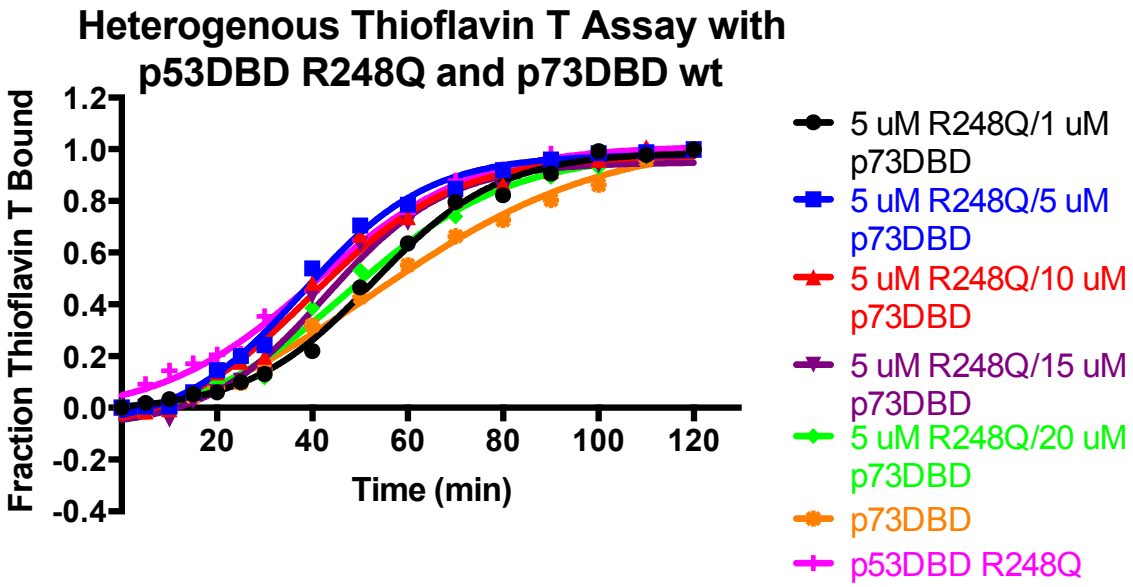

Figure 5.3. **Heterogeneous Thioflavin T Assay with R248Q p53 DBD and wild-type p73 DBD**. Thioflavin T assay was conducted with heterogeneous sample mixture consisting of 5 µM of soluble mutant R248Q p53 DBD and 1 µM wild-type p73 DBD, with 25 µM thioflavin T. Mixture was incubated at 37ºC for 2 hours. The fluorescence intensity was measured at an excitation of 450 nm and emission of 480 nm; from the fluorescence intensity values, the aggregation fraction was then calculated. Assay was repeated with varying concentrations of wild-type p73 DBD. Controls used were wild-type p73 DBD and R248Q p53 DBD by themselves.

Table 5.3. **Thioflavin$_{(t1/2)}$ Bound Values for Heterogeneous Th T Assay**. The thioflavin$_{(t1/2)}$ bound values, in minutes, was determined for each of the heterogeneous thioflavin T assay shown in Figure 5.3.

Mutant	Th$_{(t1/2)}$ Bound (min)
5 µM R248Q p53 DBD/1 µM p73 DBD	53
5 µM R248Q p53 DBD/5 µM p73 DBD	38
5 µM R248Q p53 DBD/10 µM p73 DBD	40
5 µM R248Q p53 DBD/15 µM p73 DBD	43
5 µM R248Q p53 DBD/20 µM p73 DBD	47
wild-type p73 DBD	53
R248Q p53 DBD	40

Chapter Six

Conclusions and Discussion

6.1 Conclusions

The overall conclusions of this study consist of observations that the wild-type displayed the tendency to aggregate and form amyloid fibrils. In addition, commonly cancer p53 mutations exhibited a higher propensity to form amyloid fibrils than the wild-type. Likewise, variation in amyloid fibril formation was seen amongst the p53 mutants. Structural data suggest that each mutant alters the surface of the protein in a specific manner, resulting in packing contacts unique to each mutant.

6.2 Discussion

Mutations in p53 frequently occur in the DNA binding domain, where the majority of these mutations are missense mutations (Toledo and Wahl 2006). Unlike most tumor suppressor genes that become inactive once mutated, mutated p53 has been shown to gain novel activities. These new gain of function characteristics play a role in tumorigenesis through interactions with cellular proteins (Haupt et al 2009) and transcription of various regulator genes in cancer cells (Brosh and Rotter 2009). Recent studies have shown the propensity of mutant p53 in forming amyloid fibrils, which possess prion-like behavior, capable of seeding aggregation of native p53 in the cell (Ishimaru et al. 2009). This novel occurrence provides another layer in the gain of function characteristics present in mutant p53. Previous results from a former lab member validated the presence of these amyloid fibrils in mutant p53 DBD R248Q, p53 DBD R273H, p53 DBD R248S, and wild-type p53 DBD through TEM micrographs (Lefever 2014). The shape of the amyloid fibrils present in each of the wild-type p53 DBD and their mutants varied in thickness and assembly, where some featured structured networks

of amyloid fibrils and others formed filamentous-like fibrils. The lack of uniformity amongst the mutants and the wild-type seen in the micrographs allude to subtle differences which may represent differing characteristics, behavior, and activity.

To further investigate the gain of function characteristic present in the amyloid fibrils of p53, a seeding assay was conducted using a mature fibril of mutant R248Q p53DBD to seed native wild-type p53DBD. As a control, wild-type p53 DBD displayed the propensity to form amyloid fibrils, but in a slow gradual manner (Figure 3.7 and Table 3.1). The ability to form amyloid fibrils seen in the wild-type supported previous results in the TEM micrographs. The amyloid seeding assays revealed that mature fibril R248Q p53 DBD influenced the amyloid formation of wild-type p53 DBD. According to Figure 3.7 and Table 3.1, at 10 μM of soluble p53 DBD, there was a dramatic shift in its rate of amyloid fibril formation in comparison to 5 μM p53 DBD, in which the significant shift to the left indicated a rapid amyloid formation. The increased concentration of wild-type p53 DBD allowed for more of the mature mutant R248Q fibrils to induce fibril formation onto the wild-type in comparison to having a less concentrated sample. Likewise, the growth face of the mature mutant R248Q fibrils and the soluble wild-type p53 DBD substrate share complementarity in similar structures, suggesting this attribute was an important factor in influencing the onset of fibril formation. Analysis of Figure 3.7 and Table 3.1 suggest an apparent dominant negative effect that the mature fibril R248Q p53 DBD has on the wild-type; introduction of the mutant mature fibril in the presence of soluble wild-type began to inactivate the wild-type eventually elongating the pre-existing amyloid fibril polymer.

Some of the most-frequently-mutated missense mutations in the p53 DNA binding domain have a higher propensity to form amyloid fibrils than other mutants. The order of mutation frequency is the following: R248Q, R273H, and G245S (Joerger and Fersht 2008). Structurally, the first two mutants are called contact mutants because they affect DNA binding, while the G245S mutant is called a structural mutant because it affects the folding of the protein. These mutants displayed differing rates of amyloid fibril formation in our thioflavin T fluorescence fluorescence assay (ThT assay - Figure 3.8 and Table 3.2). The ThT assays in Figure 3.2 revealed a significantly faster rate of fibril formation for the structural mutant G245S p53 DBD than the contact mutants R248Q and R273H. The rapid amyloid fibril formation of G245S highlighted its unstable characteristics, evidenced by the G245S mutant's tendency to unfold and form aggregates faster than the other p53DBD mutants. Conversely, contact mutants R248Q and R273H revealed a lower propensity for forming aggregates, with delayed rates in fibril formation.

Despite studies indicating the thermodynamic stability of contact mutants (Joerger et al 2006), the R24Q and R273H p53 DBD mutants also form aggregates. Significant differences between protein mutants were apparent in their varying propensities to form aggregates; these mutants varied in differing single amino acid mutations in the protein, yet each mutant displayed nuanced differences found in the varying rates of fibril formation. However, it is not clear whether the differing rates of fibril formation relate to altering tumorigenic behavior.

Due to its more amenable biochemical behavior, we focused our biophysical and structural characterization on the most common R248Q p53 DBD mutant. The crystal

packing of this mutant was studied together with the one for the R248S mutant to understand the filament formation at the molecular level. The structural alignment of the two crystals structures of these mutants was similar. Nonetheless, there were differences in the unit cell dimensions of both mutants that indicated differences in crystal packing that resulted in the shifted arrangement of the dimers found in the asymmetric unit of the mutants (Lefever 2014).

Further analysis of the packing through examination of their monomeric unit cells indicated greater alignment along one axis, evident in the center monomer interacting with side 2 and side 4 monomers, respectively, with an additional alignment when the center monomer interacted with the bottom monomers (Figure 4.3). This was evident when analyzing the contacts from each monomer in respect to the center monomer (Table 4.3). The differences between these two mutants within their monomeric unit cell contacts involved additional contacts present in one mutant but not the other, which occurred in each monomer pair (Table 4.1 and Table 4.2). Substantial differences in contact were present when the center monomer interacted with the top, side 1, and side 3 (Table 4.3). Despite small differences in amino acid mutations from a large and polar glutamine to a small and polar serine, packing becomes affected, present in the shift in the dimer and the monomeric unit cell. Likewise, this affirms the diversity present amongst the mutant p53 DBD, as slight differences in the amino acid mutation at the same residue position did not illicit identical characteristics.

Further studying frequently mutated residue R248, mutation of this residue to a glutamine, lysine, and serine exhibited varying amyloid fibril formation rates through the thioflavin t assays. As shown in Figure 3.9 and Table 3.3, from fastest amyloid fibril

formation to slowest, the order of mutants were the following: R248K p53 DBD, R248S p53 DBD, R248Q p53 DBD. The varying rates of fibril formation seen in the R248 mutants coincide with results in Figure 3.8 and Table 3.2 involving other common p53 DBD mutants, which affirm that minute differences in amino acid mutations can inherently display different attributes. In addition, it is uncertain why changes in R248 into a large and polar glutamine, small and polar serine, or charged and polar lysine would aggregate at differing rates.

Structural analysis of mutant R248K p53 DBD was compared against mutant R248Q p53 DBD and mutant R248S p53 DBD in order to analyze their crystal packing. Comparison of unit cell dimensions of R248K p53 DBD (Table 4.4) with R248S p53 DBD and R248Q p53 DBD displayed minor differences amongst the three mutants, yet the dimensions of R248K were more similar to R248S than R248Q. This hinted crystal packing similarities between R248K p53 DBD and R248S p53 DBD. Examination of the filamentous-like crystal packing of R248K p53 DBD (Figure 4.7) displayed similar ordered arrangement to R248S p53 DBD (Figure 4.1b) than R248Q p53 DBD (Figure 4.1a). Superimposition of the dimeric mutant R248K p53 DBD with R248S and R248Q did not easily highlight crystal packing differences (Figure 4.6), therefore the monomeric unit cell was further analyzed. Monomeric unit cell alignments of R248K p53 DBD to R248S p53 DBD and R248Q p53 DBD, respectively, displayed similar alignments between each mutant pair with slight shifts (Figure 4.7). The shift in alignment was apparent between R248K p53 DBD and R248Q p53 DBD, where their top monomers were not able to superimpose onto each other (Figure 4.7). Overall, all three R248 mutants exhibited greater alignment along one axis, specifically from the center to side 2

and side 3 monomer, respectively, as well as the bottom monomer (Table 4.7 and 4.8). The major differences setting these mutants apart are their completely different contacts unique to each mutant as well as relative contact pair similarities, where two mutants may both share a conserved residue that interacts with different residues, depending on the mutant (Table 4.1, Table 4.2, Table 4.6). Overall, varying amino acid mutations within the same residue R248 affected crystal packing.

A second mutation was introduced to hot-spot mutant R248Q, in order to determine whether mutating residue Y103 would delay fibril formation. Residue Y103 appeared to be involved in the packing of R248Q, in which residue Y103 had direct contact with residue R248Q. Residue Y103 was mutated to an alanine, lysine, or aspartate, as mutating slightly hydrophobic Y103 to a more charged residue would increase the solubility. Despite the expectations of a delayed fibril formation, introduction of a second mutation to R28Q induced fibril formation at a faster rate, as seen in Figure 5.1 and Table 5.2. In Figure 5.1, it was evident that second mutation did not stabilize the first mutation since the presence of the double mutation induced aggregation at an earlier onset compared to the R248Q control. In addition, Y103A, Y103K, Y103 mutants were used as controls and also showed a rapid emergence of aggregation. The single mutants revealed a faster fibril formation than the double mutants, indicating that there was slight stabilization in fibril formation, but not a dramatic delay. Overall, mutation at residue Y103 suggested that this residue did not stabilize the fibril formation of R248Q, as the Y103 mutation induced, rather than delayed, formation.

To further explore the behavior of Y103 mutants, it was pertinent to understand the crystal packing. Initially, the unit cell dimensions of Y103K p53 DBD (Table 4.10) hinted crystal packing differences as it varied from the unit cell dimensions of the three R248 mutants, yet it was clear that Y103K was more similar to R248Q p53 DBD, while R248K p53 DBD and R248S p53 DBD were more similar to each other in terms of unit cell dimensions. Comparison of the unit cell of Y103K (Figure 4.10) to the three R248Q mutants illustrated varying arrangement within their filamentous-like crystal packing. This was even more evident when examining their monomeric unit cell alignment, where Y103K p53 DBD similarly superimposed onto the three R248 mutants, yet it was visible that the top and bottom monomers were not able to superimpose onto each other (Figure 4.10). The most common feature in all four mutant p53 DBD monomeric unit cells was their increased common contacts found when the center monomer interacted with side 2 and side 4 monomers, respectively (Table 4.12, Table 4.13, Table 4.14). This differed from analysis of the three R248 mutants solely, where, in addition to common contacts found in these two pairs of monomers, the center to bottom monomer also shared common contacts (Table 4.7 and Table 4.8). Likewise, these common contacts along the side 2-center-side 4 axis appeared to be conserved amongst the four mutants, where contacts between the center to top, side 1, side 3, and bottom, respectively, varied between mutants. Despite the varying amyloid fibril formation rates seen in these four single amino acid surface residue mutations, the crystal packing illustrated specific conserved contacts, yet the differences highlight aspects unique to each mutant.

The gain of function characteristic of mutant p53 DBD was further studied by determining how it would interact with wild-type p73 DBD, which has been speculated to

rescue mutant p53 function. The amyloid seeding assay involving seeding mature mutant R248Q p53 DBD fibrils with soluble p73 DBD, the results revealed amyloid formation behavior differing from the wild-type. According to Figure 5.2 and Table 5.2, there was a significant onset of amyloid formation at 5 μM of p73 DBD, but at 10 μM p73 DBD there was only a slight increased in the rate of fibril formation compared to the control and delayed rate when comparing the results at 5 μM p73 DBD. Unlike the seeding assay in the presence of wild-type p53 DBD, the presence of p73 DBD at increased concentrations displayed a gradual decrease in rate of amyloid fibril formation compared to a less concentrated p73 DBD sample. The delayed rate of amyloid formation suggests the importance of complementarity between the growth face of the seed and the substrate; structural surface differences between p73 DBD and mutant R248Q suggest a key role in the ability for the fibril seed to inactivate its substrate, as well as the elongation and packing of the mature amyloid fibril.

The heterogeneous mixture of soluble mutant R248Q p53 DBD and wild-type p73 DBD revealed inconclusive results in the thioflavin T assays, suggesting a nuance in behavior when mutant p53 DBD interacts with wild-type p73 DBD. According to Figure 5.3 and Table 5.3, there was a significant increase in amyloid formation at equal concentrations of mutant R248Q p53 DBD and wild-type p73 DBD, and as the concentration of wild-type p73 DBD increased, formation began to delay. The delay in aggregation displays the importance of an increased proportion of wild-type p73 DBD in the solution as it suggests the ability for wild-type p73 DBD to stabilize the fibril forming mutant R248Q p53 DBD. This stabilization can be due to the differences in structural complementarity that is allowing surfaces on wild-type p73 DBD to interact with surfaces

on the mutant R248Q p53 DBD in such a manner that it is preventing regions in R248Q p53 DBD from unfolding. However, at 1 μM wild-type p73 DBD and 5 μM R248Q p53 DBD, this assay displayed the most significant delay in amyloid formation. It was expected that at lower proportions of wild-type p73 DBD, the dominant presence of mutant R248Q p53 DBD in the mixture would induce aggregation faster, which would be similar to the mutant R248Q p53 DBD control, but the results proved otherwise. From these results, the effects of increasing or decreasing proportions of wild-type p73 DBD in the presence of a constant concentration of mutant R248Q p53 DBD were inconclusive.

References

Aguilar, F., Hussain, S., Cerutti, P. (1993). "Aflatoxin B1 induces the transversion of G->T in codon 249 of the tumor suppressor gene in human hepatocytes." Proc Natl Acad Sci USA **90**(18): 8586-8590.

Ahn, J. and C. Prives (2001). "The C-terminus of p53: the more you learn the less you know." Nat Struct Biol **8**(9): 730-732.

Alarcon-Vargas, D. and Z. Ronai (2001). "p53-Mdm2-the affair that never ends." Carcinogenesis **23**(4): 541-547.

Ano Bom, A., Rangel, L., Costa, D., de Oliveira, G., Sanches, D., Braga, C, Gava, L, Ramos, C., Cepeda, A., Stumbo, A., De Moura Gallo, C., Cordeiro, Y., Silva, J. (2012). "Mutant p53 aggregates into prion-like amyloid oligomers and fibrils: implications for cancer." J Biol Chem **287**(33): 28152-28162.

Avantaggiati, M., Ogryzko, V., Gardner, K., Giordano, A., Levine, A., Kelly, K. (1997). "Recruitment of p300/CBP in p53-dependent signal pathways." Cell **89**(7): 1175-1184.

Baptiste, N., Friedlander, P., Chen, X., Prives, C. (2002). "The proline-rich domain of p53 is required for cooperation wih anti-neoplastic agents to promote apoptosis of tumor cells." Oncogene **21**(1): 9-21.

Biderman, L., Poyurovsky, M., Assia, Y., Manley, J., Prives, C. (2012). "MdmX is required for p53 interaction with and full induction of the Mdm2 promoter after cellular stress." Mol Cell Biol **32**(7): 1214-25.

Bosari, S., Viale, G., Bossi, P., Maggioni, M., Coggi, G., Murray, J., Lee, A. (1994). "Cytoplasmic accumulation of p53 protein: an independent prognostic indicator in colorectal adenocarcinomas." J Natl Cancer Inst **86**(9): 681-687.

Brosh, R. and V. Rotter (2009). "When mutants gain new powers: news from the mutant p53 field." Nat Rev Cancer **9**(10): 701-13.

Bullock, A., Henckel, J., DeDecker, B., Johnson, C., Nikolova, P., Proctor, M., Lane, D., Fersht, A. (1997). "Thermodynamic stability of wild-type and mutant p53 core domain." Proc Natl Acad Sci USA **94**(26): 14338-14342.

Chan, W., Siu W., Lau, A., Poon, R. (2004). "How many mutant p53 molecules are needed to inactivate a tetramer?" Mol Cell Biol **24**(8): 3536-3551.

Chene, P. (2001). "The role of tetramerization in p53 function." Oncogene **20**(21):2611-2617.

Chipuk, J., Kuwana, T., Bouchier-Hayes, L., Droin, N., Newmeyer, D., Schuler, M., Green, D. (2004). "Direct activation of Bax by p53 mediates mitochondrial membrane permeabilization and apoptosis." Science **303**(5660): 1010-1014.

Cho, Y., Gorina, S., Jeffrey, P., Pavletich, N. (1994). "Crystal structure of a p53 tumor suppressor-DNA complex: understanding tumorigenic mutations." Science **265**(5170): 346-355.

Ciribilli, Y., Monti, P., Bisio, A., Nguyen, H., Ethayathulla, A., Ramos, A., Fogetti, G., Menichini, P., Menendez, D., Resnick, M., Viadiu, H., Fronza, G., Inga, A. (2013). "Transactivation specificity is conserved among p53 family proteins and depends on a response element sequence code." Nucleic Acids Res **41**(18): 8637-8653.

Dawson, R., Muller, L., Dehner, A., Klein, C., Kessler, H., Buchner, J. (2003). "The N-terminal domain of p53 is natively unfolded." J Mol Biol **332**(5): 1131-1141.

DeLano, W. The PyMOL Molecular Graphics System, Version 1.5.0.4 Schrödinger, LLC (2004).

Di Como, C. and C. Prives (1998). "Human tumor-derived p53 proteins exhibit binding site selectivity and temperature sensitivity for transactivation in a yeast-based assay." Oncogene **16**(19): 2527-2539.

Erster, S., Mihara, M., Kim, R., Petrenko, O., Moll, U. (2004). "In vivo mitochondrial p53 translocation triggers a rapid wave of cell death in response to DNA damage that can precede p53 target gene activation." Mol Cell Biol **24**(15): 6728-6741.

Forget, K., Tremblay, G., Roucou, X. (2013). "p53 Aggregates penetrate cells and induce the co-aggregation of intracellular p53." PLoS One **8**(7): 1-9.

Freed-Pastor, W. and C. Prives (2012). "Mutant p53: one name, many proteins." Genes Dev **26**(12): 1268-1286

Harris, S.L. and A.J. Levine (2005). "The p53 pathway: positive and negative feedback loops." Oncogene **24**(17): 2899-2908.

Harrison, R., Sharpe, P., Singh, Y., Fairlie, D. (2007). "Amyloid peptides and proteins in review." Rev Physiol Biochem Pharmacol **159**: 1-77.

Haupt, S., di Agostino, S., Mizrahi, I, Alsheich-Bartok, O., Voorhoeve, M., Damalas, A., Blandino, G., Haupt, Y. (2009). Promyelocytic leukemia protein is required for gain of function by mutant p53. Cancer Res **69**(11): 4818-4826.

Ishimaru, D., Andrade, L., Teixeira, L., Quesado, P., Maiolino, L., Lopez, P., Cordeiro, Y., Costa, L., Heckl, W., Weissmuller, G., Foguel, D., Silva, J. (2003). "Fibrillar aggregates of the tumor suppressor p53 core domain." Biochemistry **42**(30): 9022-9027.

Ishimaru, D., Lima, L., Maia, L, Lopez, P., Ano Bom, A., Valente, A., Silva, J. (2004). "Reversible aggregation plays a crucial role on the folding landscape of p53 core domain." Biophys J **87**(4): 2691-2700.

Ishimaru, D., Ano Bom, A., Lima, L., Quesado, P., Oyama, M., de Moura Gallo, C., Cordeiro, Y., Silva, J. (2009). "Cognate DNA stabilizes the tumor suppressor p53 and prevents misfolding and aggregation." Biochemistry **48**(26):6126-6135.

Jeffrey, P., Gorina, S., Pavletich, N. (1995). "Crystal structure of the tetramerization domain of the p53 tumor suppressor at 1.7 angstroms." Science **267**(5203): 1498-1502.

Jenkins, L., Durell, S., Mazur, S., Apella, E. (2012). "p53 N-terminal phosphorylation: a defining layer of complex regulation." Carcinogenesis **33**(8): 1441-1449.

Joerger, A., Ang, H., Veprintsev, D., Blair, C., Fersht, A. (2005). "Structures of p53 cancer mutants and mechanism of rescue by second-site suppressor mutations." J Biol Chem **280**(16): 16030-16037.

Joerger, A.C., Ang, H.C., Fersht, A.R. (2006). "Structural basis for understanding oncogenic p53 mutations and designing rescue drugs." Proc Natl Acad Sci USA **103**(41): 15056-15061.

Joerger, A.C. and A.R. Fersht (2008). "Structural biology of the tumor suppressor p53." Annu Rev Biochem **77**: 557-582.

Joerger, A.C. and A.R. Fersht (2010). "The tumor suppressor p53: from structures to drug discovery." Cold Spring Harb Perspect Biol **2**(6): 1-20.

Kopito, R. and D. Ron (2000). "Conformational disease." Nat Cell Biol **2**(11): E207-E209.

Lasagna-Reeves, C., Clos, A., Castillo-Carranza, D., Sengupta, U., Guerrero-Munoz, M., Kelly, B., Wagner, R., Kayed, R. (2013). "Dual role of p53 amyloid formation in cancer; loss of function and gain of toxicity." Biochem Biophys Res Commun **430**(3): 963-968.

Lee, H., Mok, K., Muhandiram, R., Park, K., Suk, J., Kim, D., Chang, J., Sung, Y., Choi, K., Han, K. (2000). "Local structural elements in the mostly unstructured transactivation domain of human p53." J Biol Chem **275**(38): 29426-29432.

Lefever, K.J. (2014). "Biophysical Characterization of the p53 DNA Binding Domain Hotspot Mutations." La Jolla, University of California, San Diego.

Leslie, A.G.W. and H.R. Powell (2007). Evolving Methods for Macromolecular Crystallography, 245, 41-51 ISBN 978-1-4020-6314-5.

Levine, A.J. (1997). "p53, the cellular gatekeeper for growth and division." Cell **88** (3): 323-331.

Levine, A.J. and M. Oren (2009). "The first 30 years of p53: growing ever more complex." Nat Rev Cancer **9**(10): 749-758.

Liu, J., Zhang, C., Feng, Z. (2014). "Tumor suppressor p53 and its gain-of-function mutants in cancer." Acta Biochim Biophys Sin (Shanghai) **46**(3): 170-179.

Marchenko, M., Hanel, W., Li, D., Becker, K., Reich, N., Moll, U. (2010). "Stress-mediated nuclear stabilization of p53 is regulated by ubiquitination and importin-alpha3 binding." Cell Death Differ **17**(2): 225-267.

Meek, D. and C. Anderson (2009). "Posttranslational modification of p53: cooperative integrators of function." Cold Spring Harb Perspect Biol **1**(6): 1-16.

Momand, J., Zambetti, G., Olson, D., George, D., Levine, A. (1992). "The mdm-2 oncogene product forms a complex with the p53 protein and inhibits p53-mediated transactivation. Cell **69**(7): 1237-1245.

Pettersen, E.F., Goddard, T.D., Huang, C.C., Couch, G.S., Greenblatt, D.M., Meng, E.C., Ferrin, T.E. (2004). "UCSF Chimera-a visualization system for exploratory research and analysis." J Comput Chem **25**(13): 1605-1612.

Picksley, S.M. and D.P. Lane (1993). "The p53-mdm2 autoregulatory feedback loop: a paradigm for the regulation of growth control by p53?." Bioessays **15**(10): 689-690.

Rolley, N., Butcher, S., Milner, J. (1995). "Specific DNA binding by different classes of human p53 mutants." Oncogene **11**(4): 763-770.

Rotter, V., Abutbul, H., Ben-Ze'ev, A. (1983). "P53 transformation-related protein accumulates in the nucleus of transformed fibroblasts in association with chromatin and is found in the cytoplasm of non-transformed fibroblasts." EMBO **2**(7): 1041-1047.

Sarnow, P., Ho, Y., Williams, J., Levine, A. (1982). "Adenovirus E1b-58kd tumor antigen and SV40 large tumor antigen are physically associated with the same 54 kd cellular protein in transformed cells." Cell **28**(2): 387-394.

Song, H., Hollstein, M., Xu, Y. (2007). "p53 gain-of-function cancer mutants induce genetic instability by inactivation ATM." Nat Cell Biol **9**(5): 573-580.

Teodoro, J.G., Evans, S.K., Green, M.R. (2007). "Inhibition of tumor angiogenesis by p53: a new role for the guardian of the genome." J Mol Med **85**(11): 1175-1186.

Teufel, D., Freund, S., Bycroft, M., Fersht, A. (2007). "Four domains of p300 each bind tightly to a sequence spanning both transactivation subdomains of p53." Proc Natl Acad Sci USA **104** (17): 7009-7014.

Toledo, F. and G. Wahl. (2006). "Regulating the p53 pathway: *in vitro* hypotheses, *in vivo veritas*." Nature Reviews Cancer **6**(12): 909-923.

Venot, C., Maratrat, M., Dureuil, C., Conseiller, E., Bracco, L., Debussche, L. (1998). "The requirement for the p53 proline-rich functional domain for mediation of apoptosis is correlated with specific PIG3 gene transactivation and with transcriptional repression. EMBO J **17**(16):4668-4679.

Viadiu, H. (2008). "Molecular architecture of tumor suppressor p53." Curr Top Med Chem **8**(15): 1327-1334.

Vousden, K.H. and D.P. Lane (2009). "p53 in health and disease." Nature Rev Mol Cell Bio **8**(4): 275-283.

Wang, Y. and W. Eckhart (1992). "Phosphorylation sites in the amino-terminal region of mouse p53." Proc Natl Acad Sci USA **89**(10): 4231-4235.

Wade, M., Li, Y., Wahl, G. (2013). "MDM2, MDMX and p53 in oncogenesis and cancer therapy." Nat Rev Cancer **13**(2): 83-96.

Wolf, D., Harris, N., Rotter, V. (1984). "Reconstitution of p53 expression in a nonproducer Ab-MuLV-transformed cell line by transfection of a functional p53 gene." Cell **38**(1): 119-126.

Xu, J., Reumers, J., Couceiro, J., De Smet, F., Gallardo, R., Rudyak, S., Cornelis, A., Rozenski, J., Zwolinska, A., Marine, J., Lambrechts, D., Suh, Y., Rousseau, F., Schymkowitz, J. (2011). "Gain of function of mutant p53 by coaggregation with multiple tumor suppressors." Nat Chem Biol **7**(5): 285-295.

Xu, Y. (2003). "Regulation of p53 responses by post-translational modifications." Cell Death Differ **10**(4): 400-403.